J. Fluid Mech. (1999), *vol.* 395, *pp.* 29–59. Printed in the United Kingdom

Hydrodynamic interactions and collision efficiencies of spherical drops covered with an incompressible surfactant film

By J. BŁAWZDZIEWICZ[1,2], E. WAJNRYB[2] AND MICHAEL LOEWENBERG[1]

[1] Department of Chemical Engineering, Yale University, New Haven, CT 06520-8286, USA

[2] Institute of Fundamental Technological Research, Polish Academy of Sciences, Swiętokrzyska 21, 00-048 Warsaw, Poland

(Received 30 April 1998 and in revised form 31 March 1999)

A theory is developed for the hydrodynamic interactions of surfactant-covered spherical drops in creeping flows. The surfactant is insoluble, and flow-induced changes of surfactant concentration are small, i.e. the film of adsorbed surfactant is incompressible.

For a single surfactant-covered drop in an arbitrary incident flow, the Stokes equations are solved using a decomposition of the flow into surface-solenoidal and surface-irrotational components on concentric spherical surfaces. The surface-solenoidal component is unaffected by surfactant; the surface-irrotational component satisfies a slip-stick boundary condition with slip proportional to the surfactant diffusivity. Pair hydrodynamic interactions of surfactant-covered bubbles are computed from the one-particle solution using a multiple-scattering expansion. Two terms in a lubrication expansion are derived for axisymmetric near-contact motion.

The pair mobility functions are used to compute collision efficiencies for equal-size surfactant-covered bubbles in linear flows and in Brownian motion. An asymptotic analysis is presented for weak surfactant diffusion and weak van der Waals attraction. In the absence of surfactant diffusion, collision efficiencies for surfactant-covered bubbles are higher than for rigid spheres in straining flow and lower in shear flow. In shear flow, the collision efficiency vanishes for surfactant diffusivities below a critical value if van der Waals attraction is absent.

1. Introduction

Adsorbed surfactant affects emulsion flows by modifying interfacial stresses. The pervasive influence of surfactant on the hydrodynamic behaviour of bubbles and drops has been recognized since the early work of Frumkin & Levich (1947). Recent investigations of multiphase flows with surfactants are reviewed by Edwards, Brenner & Wasan (1991), Kralchevsky, Danov & Ivanov (1996) and Maldarelli & Huang (1996).

Surfactants introduce complex features into the dynamics of multiphase systems. These features include surfactant adsorption and desorption, nonlinear convective transport, and surfactant diffusion (e.g. Stebe & Maldarelli 1994; Chen & Stebe 1996). Drop deformation and hydrodynamic interactions between drops are affected by adsorbed surfactants. Thus, surfactants influence drop coalescence (Cristini,

Bławzdziewicz & Loewenberg 1998), drop breakup (Stone & Leal 1990; Pawar & Stebe 1996), and emulsion rheology (Yon & Pozrikidis 1998).

For sufficiently small drops or weak flows, surface tension dominates deforming viscous stresses, thus drops remain spherical. For low-viscosity fluids in creeping flows, these conditions are almost always satisfied. Adsorbed surfactants modify the hydrodynamic interactions through the coupling of viscous tangential tractions and surface-tension gradients (Marangoni stresses). Scaling arguments, shown herein, indicate that Marangoni stresses maintain nearly constant surfactant concentration on the interface of a spherical drop unless the surfactant elasticity is low. The surfactant film is thus incompressible, by analogy to the density of an incompressible fluid. Incompressibility usually holds when interface deformation is unimportant.

Herein, we study the hydrodynamic interactions of surfactant-covered spherical drops under these conditions. Marangoni stresses and surfactant diffusion are included in our analysis; surface viscosity is neglected. The surfactant is assumed to be insoluble in the bulk phases.

We solve the general problem of a single surfactant-covered drop in Stokes flow by decomposing the flow velocity into surface-solenoidal and surface-irrotational components on concentric spherical surfaces. We show that the surface-solenoidal component is unaffected by adsorbed surfactant and the surface-irrotational component satisfies a stick-slip boundary condition at the drop interface.

Pairwise mobilities are derived from the one-drop solution using a multiple-scattering technique. For axisymmetric motion, a two-term lubrication expansion is derived. The pair mobility functions are used to calculate collision efficiencies for equal-size surfactant-covered bubbles in linear flows and in Brownian motion. Asymptotic formulae are derived for weak surfactant diffusion and for weak van der Waals attraction.

The regime of incompressible surfactant films is described in § 2. There we formulate the corresponding boundary value problem for a surfactant-covered drop. A general one-drop solution is given in § 3. Pair mobility functions and collision efficiencies are presented in § 4 and § 5. Concluding remarks are given in § 6.

2. Incompressible surfactant film

We consider Stokes flow in the presence of a surfactant-covered fluid–fluid interface. The surfactant is insoluble in the bulk phases and has local interfacial concentration Γ. The local surface tension is $\sigma(\Gamma)$; surface viscosity is neglected.

Small-capillary-number conditions

$$Ca = \frac{\tau a}{\sigma_0} \ll 1 \tag{2.1}$$

are assumed, where τ is the characteristic viscous stress, a is the characteristic size of the interface, $\sigma_0 = \sigma(\Gamma_0)$, and Γ_0 is the average surfactant concentration. Thus, the interface maintains a fixed equilibrium shape.

Examples of equilibrium interfaces include spherical drops, plane interfaces, and liquid bridges. In low-viscosity fluids, condition (2.1) is almost always satisfied under low-Reynolds-number conditions.

2.1. *Limit of incompressible surfactant films*

Surfactant redistribution by an external flow generates surface-tension gradients (Marangoni stresses) that balance the jump in tangential viscous tractions across the

interface. Under some conditions, this balance is achieved with only small changes of surfactant concentration. Here we analyse this situation.

Accordingly, we expand the surface tension

$$\delta\sigma = \left(\frac{\mathrm{d}\sigma}{\mathrm{d}\Gamma}\right)_0 \delta\Gamma, \tag{2.2}$$

where $\delta\Gamma = \Gamma - \Gamma_0$ and $\delta\sigma = \sigma - \sigma_0$, and the derivative is evaluated at $\Gamma = \Gamma_0$. The result can be rewritten as

$$\frac{\delta\Gamma}{\Gamma_0} = -Ma^{-1}\frac{\delta\sigma}{\tau a}, \tag{2.3}$$

where

$$Ma = \frac{E}{Ca} \tag{2.4}$$

is the Marangoni number, and

$$E = -\frac{\Gamma_0}{\sigma_0}\left(\frac{\mathrm{d}\sigma}{\mathrm{d}\Gamma}\right)_0 \tag{2.5}$$

is the surfactant elasticity.

Marangoni stresses balance the jump in tangential viscous tractions (which scale as τ), and we assume that variations of surface tension occur over the length scale a. Thus,

$$\frac{\delta\sigma}{\tau a} = O(1) \tag{2.6}$$

and therefore,

$$\frac{\delta\Gamma}{\Gamma_0} = O(Ma^{-1}), \tag{2.7}$$

by (2.3).

In the limit

$$Ma \to \infty, \tag{2.8}$$

finite changes of surface tension correspond to infinitesimal changes of surfactant concentration, according to equations (2.6) and (2.7). Under these conditions, the surfactant film is incompressible

$$\Gamma = \Gamma_0, \tag{2.9}$$

and the surfactant concentration can be replaced by surface tension as an independent field variable in the evolution equations, provided that the system evolves on a dimensionless time scale longer than Ma^{-1}.

Incompressibility of the surfactant film is analogous to fluid incompressibility, where finite changes of pressure correspond to infinitesimal changes of fluid density, and the density is replaced by pressure as independent field variable.

According to (2.4),

$$Ma \gg 1 \tag{2.10}$$

under small-capillary-number conditions, provided that

$$E = O(1), \tag{2.11}$$

which is typical. The only exceptions correspond to interfacial phase transitions, critical points, or diluted surfactants. We conclude that under small-capillary-number conditions the surfactant film is usually incompressible.

2.2. *Governing equations*

Fluid motion on both sides of the interface is described by the Stokes equations:

$$\eta_i \nabla^2 \boldsymbol{w} - \nabla p = 0, \qquad \nabla \cdot \boldsymbol{w} = 0, \tag{2.12}$$

where $i = 1, 2$. The viscosity of the outside fluid is $\eta_1 = \eta$ and of the inside fluid is $\eta_2 = \hat{\eta}\eta_1$.

Fluid velocity is continuous across the interface,

$$\boldsymbol{w}_+ = \boldsymbol{w}_-, \tag{2.13}$$

where subscript $+$ $(-)$ denotes positions just outside (inside) the interface. In a reference frame moving with a constant-shape interface,

$$\boldsymbol{n} \cdot \boldsymbol{w} = 0 \tag{2.14}$$

on the interface, where $\boldsymbol{n}$ is the outward normal vector. In the absence of surface viscosity, the jump in tangential viscous tractions $\boldsymbol{t}$ across the interface is balanced by Marangoni stresses:

$$\boldsymbol{t}_- - \boldsymbol{t}_+ = \nabla_s \sigma, \tag{2.15}$$

where ∇_s denotes the surface gradient operator.

Surfactant flux on the interface incorporates convective and diffusive contributions:

$$\boldsymbol{j} = \Gamma_0 \boldsymbol{w} + M \nabla_s \sigma, \tag{2.16}$$

where M is the collective interfacial mobility of surfactant molecules and $\nabla_s \sigma$ is the thermodynamic force. By an Einstein argument, $D_s = -M(\mathrm{d}\sigma/\mathrm{d}\Gamma)_0$, where D_s is the surface diffusivity of the surfactant.

For insoluble surfactant, incompressibility (2.9) implies zero surface divergence of surfactant flux:

$$\nabla_s \cdot \boldsymbol{j} = 0. \tag{2.17}$$

Thus,

$$\nabla_s \cdot \left[\boldsymbol{w} + (\lambda a/\eta) \nabla_s \sigma \right] = 0, \tag{2.18}$$

where

$$\lambda = \frac{\eta M}{a \Gamma_0}. \tag{2.19}$$

Typically $\lambda \ll 1$, except for small drops and low concentrations of adsorbed surfactant.

The Stokes equations with the boundary conditions (2.13)–(2.15) and (2.18) form a well-posed boundary-value problem that has a unique solution as shown in Appendix A; the independent field variables are $(\boldsymbol{w}, \sigma)$. For incompressible surfactant films, surface tension gradients maintain a divergence-free surfactant flux on the interface. This is analogous to incompressible bulk flows, where pressure gradients maintain a divergence-free velocity field.

The regime of incompressible adsorbed films has been previously recognized by Landau & Lifshitz (1987) and Levich (1962).

3. Single spherical drop

We consider an isolated surfactant-covered drop with radius a (characteristic length). To solve the corresponding boundary-value problem (2.12)–(2.15), (2.18) we introduce the decomposition of the vector field $\boldsymbol{u}$ into surface-irrotational and

surface-solenoidal components

$$\boldsymbol{u} = \boldsymbol{u}^{\mathrm{irr}} + \boldsymbol{u}^{\mathrm{sol}} \tag{3.1}$$

on a family of concentric spherical surfaces, where

$$\boldsymbol{n} \cdot \left(\nabla_s \times \boldsymbol{u}^{\mathrm{irr}}\right) = 0, \tag{3.2}$$

and

$$\nabla_s \cdot \boldsymbol{u}^{\mathrm{sol}} = 0, \qquad \boldsymbol{n} \cdot \boldsymbol{u}^{\mathrm{sol}} = 0. \tag{3.3}$$

A similar decomposition of the velocity field is also useful for interfaces with other geometries, e.g. plane interfaces (Bławzdziewicz, Cristini & Loewenberg 1999).

The fields $\boldsymbol{u}^{\mathrm{sol}}$ and the tangential component of $\boldsymbol{u}^{\mathrm{irr}}$ are derivable from scalar potentials χ and ψ:

$$\boldsymbol{u}^{\mathrm{irr}} = \nabla_s \chi + (\boldsymbol{u} \cdot \boldsymbol{n})\boldsymbol{n}, \tag{3.4}$$

$$\boldsymbol{u}^{\mathrm{sol}} = \boldsymbol{n} \times \nabla_s \psi. \tag{3.5}$$

Decomposition (3.1) is the surface analogue of the Helmholtz decomposition for a three-dimensional vector field and is uniquely defined on any closed simply connected surface, as shown in Appendix B.

From (3.4)–(3.5) it can be shown that for a surface-irrotational (surface-solenoidal) $\boldsymbol{w}$, the field $\nabla^2 \boldsymbol{w}$ is also surface irrotational (surface solenoidal) on spherical surfaces. It follows that for any $\boldsymbol{w}$ that satisfies (2.12), the surface-irrotational and surface-solenoidal components each satisfy Stokes equations independently:

$$\eta_i \nabla^2 \boldsymbol{w}^{\mathrm{irr}} - \nabla p = 0, \qquad \nabla \cdot \boldsymbol{w}^{\mathrm{irr}} = 0; \tag{3.6}$$

$$\nabla^2 \boldsymbol{w}^{\mathrm{sol}} = 0, \qquad \nabla \cdot \boldsymbol{w}^{\mathrm{sol}} = 0. \tag{3.7}$$

Moreover, surface tractions $\boldsymbol{t}^{\mathrm{irr}}$ ($\boldsymbol{t}^{\mathrm{sol}}$) associated with $\boldsymbol{w}^{\mathrm{irr}}$ ($\boldsymbol{w}^{\mathrm{sol}}$) are surface irrotational (surface solenoidal). Thus, (2.15) and uniqueness of decomposition (3.1) imply that

$$\boldsymbol{t}_-^{\mathrm{irr}} - \boldsymbol{t}_+^{\mathrm{irr}} = \nabla_s \sigma, \tag{3.8}$$

$$\boldsymbol{t}_-^{\mathrm{sol}} - \boldsymbol{t}_+^{\mathrm{sol}} = 0. \tag{3.9}$$

Finally, (3.3) and (3.4) imply that boundary condition (2.18) reduces to

$$\boldsymbol{w}^{\mathrm{irr}} + (\lambda a/\eta)\nabla_s \sigma = 0. \tag{3.10}$$

Equations (3.6)–(3.10) indicate that the surface-irrotational and surface-solenoidal velocity fields are decoupled.

The foregoing decomposition reduces the problem into familiar subproblems. The surface-solenoidal velocity field satisfies the boundary condition corresponding to a drop with a clean interface according to (3.9). In the absence of surfactant diffusion ($\lambda = 0$), the surface-irrotational field satisfies the stick (rigid sphere) boundary condition according to (3.10); for a bubble ($\hat{\eta} = 0$) covered with a diffusing surfactant, $\boldsymbol{w}^{\mathrm{irr}}$ satisfies the slip-stick boundary condition

$$\boldsymbol{w}^{\mathrm{irr}} = (\lambda a/\eta)\boldsymbol{t}_+^{\mathrm{irr}} \tag{3.11}$$

on the bubble interface. General solutions for these cases are known (e.g. Cichocki, Felderhof & Schmitz 1988), and have natural representations in terms of surface-irrotational and surface-solenoidal components, as shown in Appendix C. The general surface-irrotational solution for a viscous drop covered with diffusing surfactant is unavailable; the solution is derived in Appendix C.

The above results have immediate application to the hydrodynamic interactions between two drops. Axisymmetric azimuthal flows are surface solenoidal on the surface of each drop; thus, surfactant-covered drops rotating about a common axis behave like drops with clean interfaces. Axisymmetric flows with zero azimuthal velocity are surface irrotational on the surface of each drop; thus in the absence of surfactant diffusion, surfactant-covered drops translating along a common axis behave like rigid spheres. Both types of surface flows are generated by transversal motion of surfactant-covered drops: the behaviour is therefore distinct from that of rigid spheres and drops with clean interfaces. A more detailed analysis of pairwise interactions between drops follows.

4. Hydrodynamic interactions of two drops

4.1. *Mobility functions*

In this section, we describe calculations for the pair-mobility functions of drops covered with an incompressible film of diffusing surfactant.

We consider the relative translational motion of two drops embedded in an ambient linear flow with strain-rate tensor

$$\boldsymbol{E} = \tfrac{1}{2}[(\nabla \boldsymbol{w}_0) + (\nabla \boldsymbol{w}_0)^{\dagger}] \tag{4.1}$$

and angular velocity

$$\boldsymbol{\omega} = \tfrac{1}{2}\nabla \times \boldsymbol{w}_0. \tag{4.2}$$

External forces $\boldsymbol{F}_i$, $i = 1, 2$ are applied to the drop centres; no torques act on the drops. By symmetry, the relative velocity of identical drops is (Batchelor & Green 1972*b*)

$$\begin{aligned}\boldsymbol{U}_{12}(\boldsymbol{r}_{12}) = \boldsymbol{\omega} \times \boldsymbol{r}_{12} + \boldsymbol{E} \cdot \boldsymbol{r}_{12} - [A(R)\hat{\boldsymbol{r}}_{12}\hat{\boldsymbol{r}}_{12} + B(R)(\hat{\boldsymbol{I}} - \hat{\boldsymbol{r}}_{12}\hat{\boldsymbol{r}}_{12})] \cdot \boldsymbol{E} \cdot \boldsymbol{r}_{12} \\ + 2\mu_1[G(R)\hat{\boldsymbol{r}}_{12}\hat{\boldsymbol{r}}_{12} + H(R)(\hat{\boldsymbol{I}} - \hat{\boldsymbol{r}}_{12}\hat{\boldsymbol{r}}_{12})] \cdot \boldsymbol{F}_{12},\end{aligned} \tag{4.3}$$

where $\boldsymbol{r}_{12}$ is the relative position of drop centres, $\hat{\boldsymbol{r}}_{12} = \boldsymbol{r}_{12}/r_{12}$, μ_1 is the mobility coefficient for an isolated drop, and $\boldsymbol{F}_{12} = \frac{1}{2}(\boldsymbol{F}_1 - \boldsymbol{F}_2)$. The scalar pair-mobility functions A, B, G, H depend only on $R = \frac{1}{2}r_{12}/a$. For a surfactant-covered drop the friction coefficient $\zeta_1 = \mu_1^{-1}$ is given by (C 49).

4.2. *Numerical results*

Mobility functions A, B, G, and H were calculated for equal-size bubbles ($\hat{\eta} = 0$) covered with an incompressible film of diffusing surfactant using the single-drop solution (described in § 3 and Appendix C) and the multiple-scattering procedure of Cichocki *et al.* (1988) (as described in Appendix D). The results are shown in figures 1–4 as functions of gap width $\epsilon = 2(R-1)$ for several values of the surfactant diffusion parameter

$$\Lambda = \frac{\lambda}{1 + 3\lambda}, \tag{4.4}$$

where $\Lambda = 0$ corresponds to non-diffusing surfactant and $\Lambda = \frac{1}{3}$ corresponds to a clean interface.

The radial mobility functions A and G are shown in figures 1 and 2. In the absence of surfactant diffusion ($\Lambda = 0$), the radial mobilities for surfactant-covered bubbles are the same as for rigid spheres, consistent with the discussion in the last

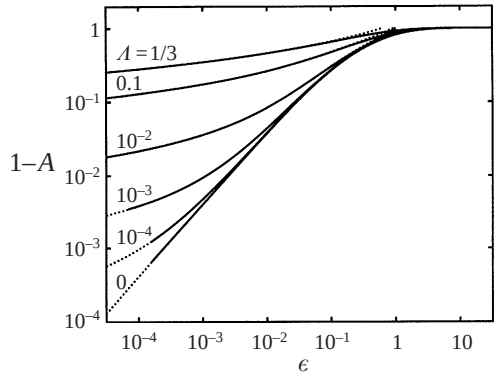

FIGURE 1. Radial mobility function $1-A$ versus gap width for bubbles covered with an incompressible film of diffusing surfactant. Surfactant diffusion parameter Λ, as labelled; for $\Lambda = 0$, the rigid-sphere mobility is obtained. Expansion in $1/R$ (solid curves); lubrication results (dotted curves).

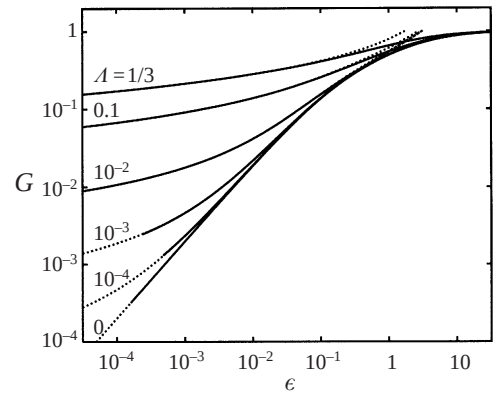

FIGURE 2. Same as figure 1 but for radial mobility function G.

paragraph of § 3. For weak surfactant diffusion, A and G differ from rigid-sphere mobilities by $O(\Lambda)$. For $\epsilon < \Lambda$, surfactant diffusion provides a logarithmic cutoff from the $O(\epsilon)$ rigid-sphere lubrication behaviour. A detailed analysis of the near-contact motion between surfactant-covered bubbles in presented in § 4.3. The $1/R$-expansion converges well except for small ϵ and Λ; the results are plotted where the convergence is better than 1%.

For axisymmetric motion, diffusion of adsorbed surfactant is analogous to Maxwell slip for rigid spheres in a rarefied gas, as indicated by (3.11). Radial mobilities for rigid spheres with Maxwell slip were obtained by Reed & Morrison (1974).

The transverse mobility functions B and H are shown in figures 3 and 4. Surfactant modifies the transverse motion of bubbles. However, in contrast to the radial mobilities, the transverse mobilities for surfactant-covered bubbles and for rigid spheres are distinct even in the absence of surfactant diffusion. The resistance functions reveal that, unlike rigid spheres, surfactant-covered bubbles in contact slide past each other, similar to bubbles with clean interfaces (Kim & Karrila 1991). For $\epsilon \to 0$, B and H tend linearly to values which depend on surfactant diffusivity (transverse mobilities of rigid spheres approach limiting values logarithmically). Contact values of B and H for several values of Λ are given in table 1. At large separations, the mobility

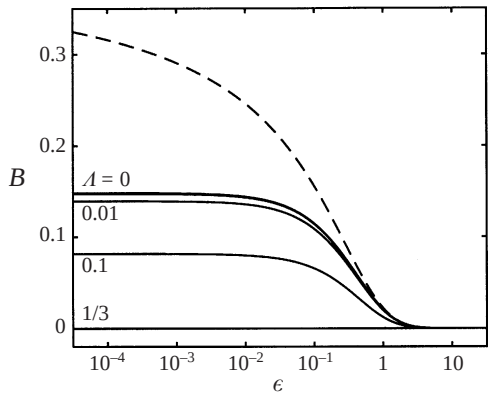

FIGURE 3. Transverse mobility function B versus gap width for bubbles covered with an incompressible film of diffusing surfactant. Surfactant diffusion parameter Λ as labelled. Surfactant-covered bubbles (solid curves); rigid spheres (dashed curve). $B = 0$ for bubbles with clean interfaces ($\Lambda = \frac{1}{3}$). Results for $\Lambda = 10^{-3}$ (unlabelled) and $\Lambda = 0$ are nearly indistinguishable.

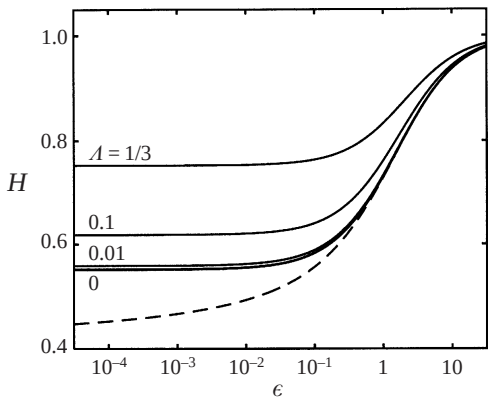

FIGURE 4. Same as in figure 3 but for transverse mobility function H.

Λ	0.0	0.0001	0.001	0.01	0.02	0.05	0.1	0.2	0.3	$\frac{1}{3}$
$B(1)$	0.14811	0.1480	0.1471	0.1392	0.1312	0.1102	0.08159	0.03904	0.008414	0
$H(1)$	0.55117	0.5513	0.5520	0.5588	0.5660	0.5863	0.6181	0.6776	0.7342	0.7527
D	2.0387	2.0386	2.0376	2.0270	2.0150	1.9783	1.9158	1.7934	1.6802	1.6449
C	1.3456	1.3453	1.3422	1.3228	1.305	1.261	1.206	1.1493	1.1895	1.2704

TABLE 1. Contact values of mobility functions B, H and lubrication constants C, D in (4.12) and (4.15) for different values of the surfactant diffusion parameter Λ.

functions B for bubbles with non-diffusing surfactant and for rigid spheres agree up to $O(R^{-7})$ and the mobility functions H agree up to $O(R^{-5})$.

4.3. *Lubrication analysis*

Mobility functions A and G were evaluated at small gaps using the results of the lubrication analysis presented in Appendix E. Accordingly, the friction coefficient

$\zeta_G = G^{-1}$ has the expansion

$$\zeta_G = \frac{\zeta_1^{HS}}{\zeta_1}[\zeta_G^{(0)} + \zeta_G^{(1)} + O(1)] \tag{4.5}$$

for

$$\bar{\delta} = \frac{6\lambda}{\epsilon} \tag{4.6}$$

held constant, where $\zeta_1^{HS} = 6\pi\eta a$ and

$$\frac{\zeta_1^{HS}}{\zeta_1} = \frac{1}{1-\Lambda} \tag{4.7}$$

according to (C 49). The first two terms in the lubrication expansion are

$$\zeta_G^{(0)} = \frac{1}{\epsilon}\left[\frac{1}{\bar{\delta}^2}\left(1+\bar{\delta}\right)\ln\left(1+\bar{\delta}\right) - \frac{1}{\bar{\delta}}\right], \tag{4.8}$$

$$\zeta_G^{(1)} = \frac{1}{60}\left[\frac{-17+20\bar{\delta}+\frac{103}{3}\bar{\delta}^2}{\bar{\delta}\left(1+\bar{\delta}\right)} + \frac{17+30\bar{\delta}-7\bar{\delta}^2}{\bar{\delta}^2}\ln(1+\bar{\delta}) + 27\ln\epsilon^{-1}\right]. \tag{4.9}$$

Lubrication formulae (4.5)–(4.9) also describe near-contact motion of rigid spheres with Maxwell slip; the leading-order contribution $\zeta_G^{(0)}$ was obtained by Hocking (1973).

Rigid-sphere lubrication (Kim & Karrila 1991) is recovered for $\lambda \to 0$,

$$\zeta_G^{(0)} = \frac{1}{2\epsilon}, \qquad \zeta_G^{(1)} = \tfrac{9}{20}\ln\epsilon^{-1} + O(1), \tag{4.10}$$

and surfactant diffusion provides a lubrication cutoff for $\epsilon \ll \lambda$,

$$\zeta_G^{(0)} = \frac{1}{6\lambda}\ln\epsilon^{-1} + O(\lambda^{-1}\ln\lambda), \qquad \zeta_G^{(1)} = \tfrac{1}{3}\ln\epsilon^{-1} - \tfrac{7}{60}\ln\lambda + O(1). \tag{4.11}$$

The near-contact lubrication resistance between surfactant-covered bubbles is accurately described by

$$\zeta_{GL}(\epsilon,\lambda) = \frac{\zeta_1^{HS}}{\zeta_1}[\zeta_G^{(0)}(\epsilon,\lambda) + \zeta_G^{(1)}(\epsilon,\lambda) - \zeta_G^{(1)}(1,\lambda)] + C(\lambda), \tag{4.12}$$

where C is independent of the gap width. Values for C, obtained by matching to our numerical results, are given in table 1 for several values of the surfactant diffusion parameter Λ. For $\Lambda = 0$ and $\Lambda = \frac{1}{3}$, our values for C agree with the result reported for rigid spheres and the exact value for bubbles with clean interfaces $C = \gamma_E + \ln 2$, where γ_E is Euler's constant (Kim & Karrila 1991).

According to our numerical calculations,

$$\zeta_G(\epsilon,\lambda) - \zeta_{GL}(\epsilon,\lambda) = \epsilon(E_1\ln\epsilon + E_2) \tag{4.13}$$

for $\epsilon \ll \lambda$, where E_1 and E_2 depend only on λ. For $\lambda \ll \epsilon \ll 1$, the same form applies but with different E_1 and E_2, and the result agrees with higher-order terms in the rigid-sphere lubrication solution (Kim & Karrila 1991). The residual behaviours are illustrated in figure 5. A lubrication formula accurate to 1% for $\epsilon < 3$ (0.1% for $\epsilon \leqslant 0.9$) is obtained for bubbles with clean interfaces using (4.12)–(4.13) with $C = \gamma_E + \ln 2$ and $E_1 = -0.083450$, $E_2 = 0.26662$.

The lubrication approximation $G_L = \zeta_{GL}^{-1}$ is shown in figure 2. In figure 1, we show the lubrication approximation

$$1 - A_L(R) = DG_L(R), \tag{4.14}$$

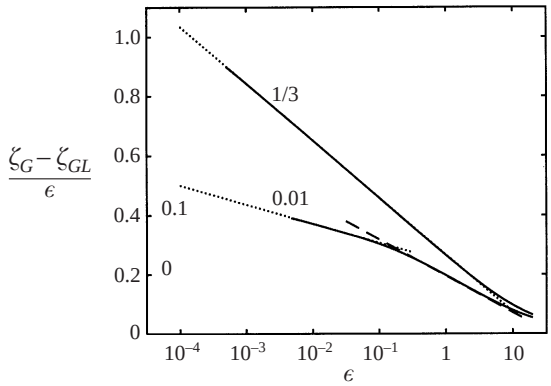

FIGURE 5. Plots of $(\zeta_G - \zeta_{GL})/\epsilon$ as a function of gap width for $\Lambda = 0.01$ and $\Lambda = \frac{1}{3}$ (as labelled). Exact results (solid curves); approximation (4.13) for $\epsilon \ll \Lambda$ (dotted lines); approximation (4.13) with hard-sphere parameters (dashed line).

where

$$D = \lim_{R\to 1} \frac{1 - A(R)}{G(R)}, \tag{4.15}$$

which is non-singular and can be accurately evaluated from the $1/R$-expansion. Numerical results for D are given in table 1.

5. Collision efficiencies

Coalescence rates in dilute suspensions of spherical drops with clean interfaces were computed by Zinchenko (1982, 1984), Zhang & Davis (1991) and Wang, Zinchenko & Davis (1994). Here we present results for equal-size bubbles covered with an incompressible film of diffusing surfactant; the effects of van der Waals attraction are included. Coalescence rates are computed for bubbles in straining flow, shear flow, and in Brownian motion.

Collision efficiencies are defined:

$$E = J/J_0, \tag{5.1}$$

where J is the actual coalescence rate and J_0 is the coalescence rate for non-interacting spheres. For equal-size spheres with radius a and number density n, $J_0 = \frac{64}{3\sqrt{3}}\pi n^2 \dot\gamma a^3$ in straining flow and $J_0 = \frac{32}{3} n^2 \dot\gamma a^3$ in shear flow, where $\dot\gamma$ is the strain or shear rate. For Brownian motion, $J_0 = 16\pi n^2 a D_B$, where D_B is the Stokes–Einstein diffusivity.

Van der Waals attraction was calculated from the approximate formula of Zinchenko & Davis (1994), which incorporates the effect of electromagnetic retardation and reduces to the two-sphere formula of Hamaker (1931) when retardation is unimportant. The strength of van der Waals attraction is characterized by

$$Q = \frac{\dot\gamma a^2}{2\mu_1 A_H}, \tag{5.2}$$

where A_H is the Hamaker constant and μ_1 is the one-particle mobility. Electromagnetic retardation is characterized by

$$v_L = \lambda_L / a, \tag{5.3}$$

where λ_L is the London wavelength. For $\epsilon \ll 1$, the unretarded van der Waals

potential Φ has the limiting behaviour

$$\Phi = -\frac{A_H}{12\epsilon}, \qquad \epsilon \ll v_L, \tag{5.4}$$

and the fully retarded van der Waals potential has the limiting behaviour

$$\Phi \sim \frac{A_H v_L}{\epsilon^2}, \qquad \epsilon \gg v_L. \tag{5.5}$$

5.1. *Non-Brownian surfactant-covered bubbles in linear flows*

5.1.1. *Axisymmetric straining flow*

In the absence of the van der Waals attraction, collision efficiencies for surfactant-covered bubbles were calculated from (Zinchenko 1984)

$$E_{st} = \mathrm{e}^{-3I_{st}(1)}, \tag{5.6}$$

where

$$I_{st}(R) = \int_R^\infty \frac{A(t) - B(t)}{1 - A(t)} \frac{\mathrm{d}t}{t}. \tag{5.7}$$

In the absence of surfactant diffusion ($\Lambda = 0$), the axisymmetric mobility $1 - A$ is proportional to gap, and thus collision efficiencies vanish according to the above formula. Surfactant diffusion provides a cutoff of the rigid-sphere lubrication resistance at

$$\epsilon^* = \Lambda, \qquad \Lambda \ll 1 \tag{5.8}$$

according to (4.8), (4.14), and the results in figure 1. An asymptotic analysis based on this observation is presented in Appendix F.

In § F.1.1, we show that

$$E_{st} = \Gamma_1 \epsilon^{*3\beta}, \qquad \epsilon^* \ll 1, \tag{5.9}$$

where β is given by (F 6) in terms of contact values of the mobility functions; the constant Γ_1 is obtained by numerical integration. For equal-size surfactant-covered bubbles, the numerical value of β is given by (F 7) and $\Gamma_1 = 0.9186$.

The effect of weak van der Waals attraction is similar to the weak surfactant diffusion: the attractive force provides a lubrication cutoff but does not influence the particle motion at large distances. An estimate for the cutoff is obtained from a balance of the hydrodynamic force $\eta\dot{\gamma}a^2$ and the (unretarded) van der Waals force obtained from (5.4):

$$\epsilon^* = Q^{-1/2} \text{ for } Q^{-1/2} \ll v_L. \tag{5.10}$$

The limiting behaviour for $Q \to \infty$ is given by (5.9)–(5.10), according to the analysis presented in § F.1.2. For equal-size surfactant-covered bubbles, $\Gamma_1 = 0.5983$ is obtained by matching to numerical results. A similar analysis using (5.5) yields (5.9) with

$$\epsilon^* = \left(Q/v_L\right)^{-1/3}, \qquad 1 \gg Q^{-1/2} \gg v_L, \tag{5.11}$$

indicating that collision efficiencies are less sensitive to van der Waals attraction in this intermediate regime.

The dependence of the collisional efficiency on the surfactant diffusion parameter (no van der Waals attraction) is depicted in figure 6. The integral (5.7) was evaluated numerically with the mobility functions A and B obtained as described in § 4. The asymptotic approximation (5.8)–(5.9) is accurate to 3% over the entire range of the surfactant diffusion parameter; the agreement for $\Lambda = O(1)$ is fortuitous.

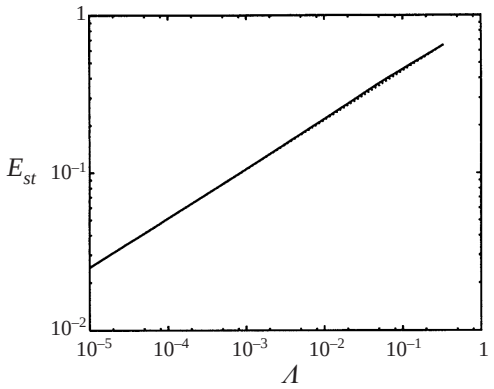

FIGURE 6. Collision efficiencies for equal-size surfactant-covered bubbles in straining flow versus surfactant diffusion parameter (van der Waals attraction absent). Numerical results (solid curve); asymptotic formula (5.9) (dotted curve). (Two curves nearly indistinguishable.)

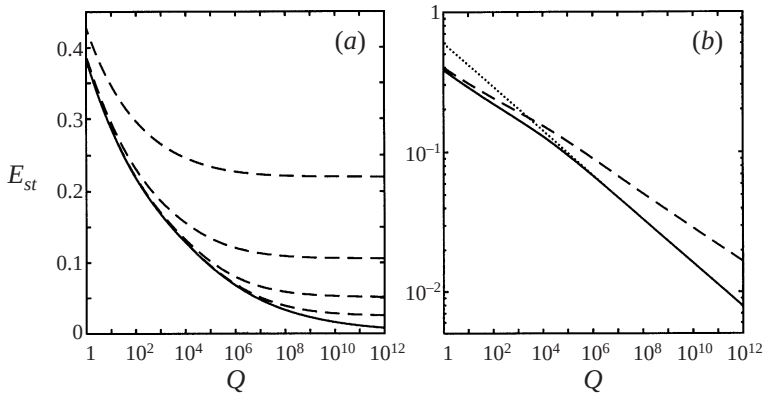

FIGURE 7. Collision efficiencies in straining flow versus van der Waals force parameter ($v_L = 0.01$): (*a*) for equal-size surfactant-covered bubbles with different values of surfactant diffusion parameter Λ (dashed curves) and $\Lambda = 0$ (solid curve); (*b*) for equal-size surfactant-covered bubbles with $\Lambda = 0$ (solid curve) and rigid spheres (dashed curve); asymptotic formula (5.9) for unretarded van der Waals attraction (dotted curve).

In the presence of van der Waals attraction collisional efficiencies were obtained by numerical integration of the relative pair trajectory backwards from the stagnation point (Wang *et al.* 1994). The dependence of the collisional efficiency on the strength of the van der Waals attraction is illustrated in figure 7. Van der Waals retardation parameter $v_L = 0.01$ was used, which corresponds to 10 μm bubbles, given a London wavelength $\lambda_L = 0.1$ μm. Collision efficiencies are controlled by the larger of the two cutoff gap widths that result from surfactant diffusion and van der Waals attraction. Thus, collision efficiencies become independent of van der Waals attraction for $Q \gg \Lambda^{-2}$, as illustrated in figure 7(*a*).

Figure 7(*b*) compares the collision efficiencies for rigid spheres and bubbles covered with non-diffusing surfactant. The transition for $Q \approx v_L^{-2}$ corresponds to the crossover between (5.10) and (5.11). The results show that collision efficiencies for surfactant-covered bubbles are lower than for rigid spheres. This result can be explained: the radial mobilities of rigid spheres and bubbles are identical; however surfactant-covered bubbles spend less time in the compressional portion of the flow because the

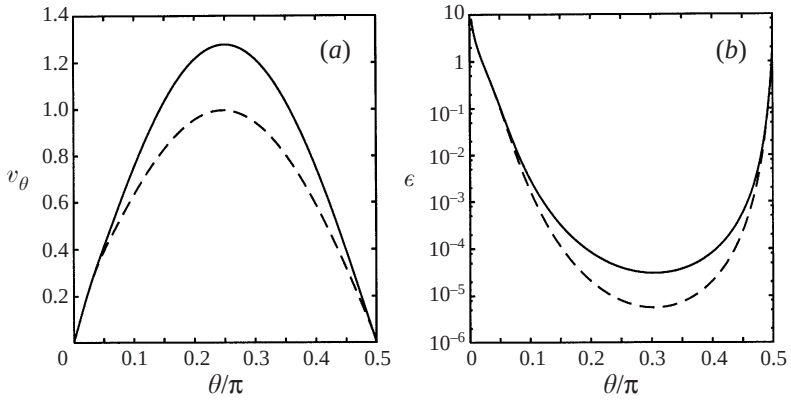

FIGURE 8. A relative trajectory in straining flow (van der Waals attraction absent). Transversal velocity (*a*) and gap width (*b*) versus angle θ with respect to strain axis. Equal-size surfactant-covered bubbles without surfactant diffusion (solid curves); rigid spheres (dashed curves).

tangential mobility is higher. Thus, surfactant-covered bubbles approach less closely. The relative motion of bubble and particle pairs is illustrated in figure 8.

5.1.2. *Shear flow*

In the absence of van der Waals attraction, collision efficiencies are given by (Zinchenko 1984)

$$E_{sh} = [E_{st}^{2/3} - I_{sh}(1)]^{3/2}, \quad E_{st}^{2/3} \geqslant I_{sh}(1), \tag{5.12}$$

$$E_{sh} = 0, \quad E_{st}^{2/3} \leqslant I_{sh}(1), \tag{5.13}$$

where

$$I_{sh}(R) = \int_R^\infty \frac{tB(t)}{1 - A(t)} \mathrm{e}^{-2I_{st}(t)}\, \mathrm{d}t, \tag{5.14}$$

and E_{st} and I_{st} are defined by (5.6) and (5.7). Equations (5.12) and (5.14) indicate that $E_{sh} \leqslant E_{st}$; for $\Lambda = \frac{1}{3}$, we have $B = 0$, thus $E_{sh} = E_{st}$.

Equation (5.13) defines the critical surfactant diffusion parameter Λ_0 such that $E_{sh} = 0$ for $\Lambda < \Lambda_0$. Collision efficiencies vanish because a region of finite trajectories, bounded by a surface Ω, encloses the entire collision surface $R = 1$ (Zinchenko 1984). Numerical solution of inequality (5.13) yields

$$\Lambda_0 = 1.9269 \times 10^{-5} \tag{5.15}$$

for equal-size surfactant-covered bubbles. The minimum thickness of the bounded-trajectory envelope is

$$\epsilon_{\min} = 2.5824 \times 10^{-5}, \tag{5.16}$$

which is comparable to the result $\epsilon_{\min} = 4.2 \times 10^{-5}$ for equal-size rigid spheres (Arp & Mason 1977). Consistent with (5.8), $\Lambda_0 \approx \epsilon_{\min}$. Larger Λ_0 and $\epsilon_{\min}$ are expected for unequal size particles (Wang *et al.* 1994).

In § F.2.1, we find the asymptotic behaviour

$$E_{sh} = \Gamma_2(\Lambda^{2\beta} - \Lambda_0^{2\beta})^{3/2} \text{ for } \Lambda \ll 1, \tag{5.17}$$

where β, Γ_2, and Λ_0 are given by (F 6), (F 33), and (F 34). For equal-size surfactant-covered bubbles, the numerical value of β is given by (F 7), $\Gamma_2 = 1.0409$, and asymptotic expression (F 34) recovers the value (5.15) with accuracy 0.3 %.

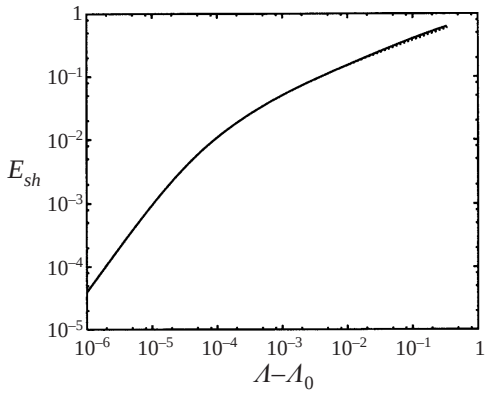

FIGURE 9. Collision efficiencies for equal-size surfactant-covered bubbles in shear flow as a function of surfactant diffusion parameter (van der Waals attraction absent). Numerical results (solid curve); asymptotic formula (5.17) (dotted curve). (Two curves nearly indistinguishable.)

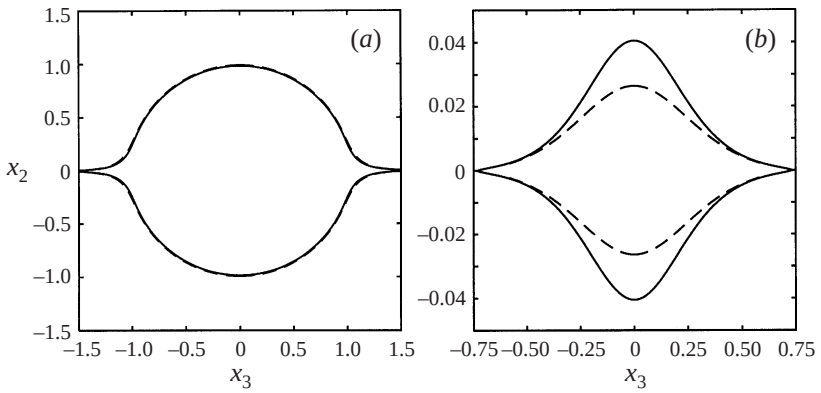

FIGURE 10. Upstream interception surfaces in shear flow. Equal-size surfactant-covered bubbles without surfactant diffusion (solid curves); rigid spheres (dashed curves). (*a*) $Q = 10^3$ and (*b*) $Q = 10^{10}$.

Non-zero van der Waals attraction causes trajectories within Ω to spiral inwards to the collision surface. Thus, closed trajectories do not exist and collision efficiencies do not vanish.

According to the analysis in § F.2.2, the asymptotic behaviour of E_{sh} is

$$E_{sh} = \Gamma_3 Q^{-1}, \quad Q^{-1/2} \ll \epsilon_{\min}, \tag{5.18}$$

for $\Lambda < \Lambda_0$. By matching to numerical results, we find $\Gamma_3 = 5.662 \times 10^5$ for equal-size bubbles covered with non-diffusing surfactant.

Collisional efficiency for surfactant-covered bubbles in shear flow (without van der Waals attraction) is plotted in figure 9 as a function of the surfactant diffusion parameter Λ. Asymptotic formula (5.17) is accurate to 8%.

For finite van der Waals attraction, collision efficiencies were obtained by integration over the upstream interception surface. The interception surface was found by integrating trajectories backwards from a downstream contour on the surface Ω, outside the range of van der Waals attraction (Wang *et al.* 1994). Examples of upstream interception surfaces are shown in figure 10. The results indicate that the interception

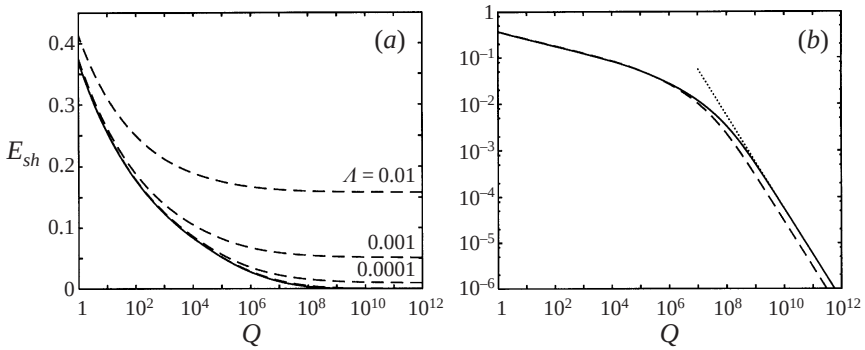

FIGURE 11. Collision efficiencies in shear flow versus van der Waals force parameter ($v_L = 0.01$); (*a*) for equal-size surfactant-covered bubbles with different values of surfactant diffusion parameter Λ (dashed curves) and $\Lambda = 0$ (solid curve) [results for $\Lambda = 10^{-5}$ (unlabelled) and $\Lambda = 0$ nearly indistinguishable]; (*b*) for equal-size surfactant-covered bubbles with $\Lambda = 0$ (solid curve) and rigid spheres (dashed curve), asymptotic formula (5.18) (dotted curve).

surface becomes elongated with a bias towards slow trajectories for weak van der Waals attraction.

The dependence of the collisional efficiency on the strength of the van der Waals attraction is illustrated in figure 11. Van der Waals retardation parameter $v_L = 0.01$ was used. As for straining flow (cf. figure 7*a*), collision efficiencies in shear flow are controlled by the larger of the two cutoff gap widths that result from surfactant diffusion and van der Waals attraction as seen in figure 11(*a*). For shear flow surfactant diffusion has only a negligible effect for $\Lambda \ll \Lambda_0$.

Figure 11(*b*) compares the collision efficiencies for rigid spheres and bubbles covered with non-diffusing surfactant. Asymptotic formula (5.18) describes collision efficiencies for $Q > \epsilon_{\min}^{-2}$. For strong van der Waals attraction, surfactant-covered bubbles have slightly smaller collision efficiencies than rigid spheres. However, in contrast to straining flow (cf. figure 7*b*), surfactant-covered bubbles in shear flow have larger collisional efficiencies for weak van der Waals attraction (1.89 times larger for $Q \to \infty$). Both observations are consistent with the results shown in figure 10.

The trajectory in figure 12 shows that surfactant-covered bubbles have higher tangential velocities than rigid spheres for $\pi/4 < \theta < 3\pi/4$ and lower tangential velocities outside this range, where θ is the angle with respect to the shear flow velocity. The net result is that surfactant-covered bubbles pass closer to the collision surface than rigid spheres.

5.2. *Brownian motion*

Collision efficiencies for Brownian motion are computed from (Spielman 1970)

$$E_B = \frac{1}{I_B(1)}, \tag{5.19}$$

with

$$I_B(R) = \int_R^\infty \frac{\exp\left(\Phi(t)/kT\right)}{t^2 G(t)}\,\mathrm{d}t, \tag{5.20}$$

where k is Boltzmann's constant and T is temperature.

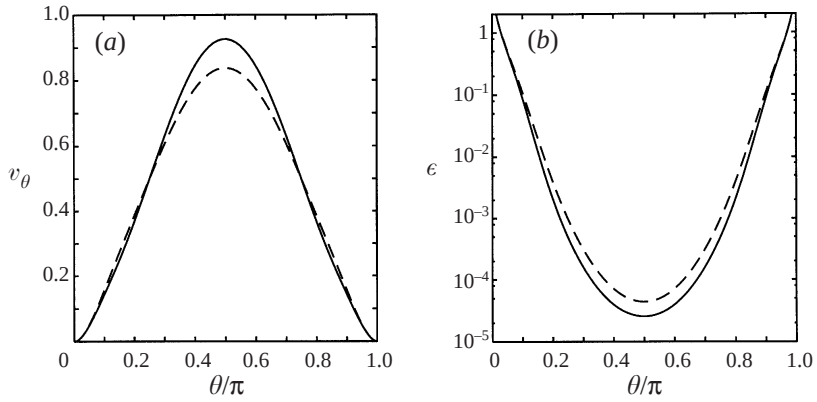

FIGURE 12. Relative trajectory in shear flow (van der Waals attraction absent). Trajectory is in the shear plane, on the envelope of finite trajectories. Transversal velocity (*a*) and gap width (*b*) versus angle θ with respect to flow direction. Equal-size surfactant-covered bubbles without surfactant diffusion (solid curves); rigid spheres (dashed curves).

By the analysis in § F.3,

$$E_B = \frac{4}{-\ln \epsilon^* + \Gamma_4}, \qquad \epsilon^* \ll 1 \tag{5.21}$$

for weak surfactant diffusion and no van der Waals attraction, where ϵ^* is the diffusive lubrication cutoff (5.8). For equal-size surfactant-covered bubbles numerical integration yields $\Gamma_4 = 5.3228$. For $\Lambda = 0$ and weak unretarded van der Waals attraction (5.4), asymptotic formula (5.21) applies with cutoff

$$\epsilon^* = \frac{A_H}{kT}. \tag{5.22}$$

For equal-size surfactant-covered bubbles, $\Gamma_4 = 7.5220$.

Collision efficiencies for Brownian motion as a function of the surfactant diffusion parameter Λ and as a function of the strength of van der Waals attraction are depicted in figure 13. The asymptotic result (5.21) (with (5.8) or (5.22)) is also shown.

According to (5.19) and (5.20), collision efficiencies for Brownian motion depend only on mobility function G; thus, the results in figure 13 apply also to rigid spheres with Maxwell slip Λ.

6. Conclusions

A theoretical description has been developed for hydrodynamic interactions of surfactant-covered spherical drops under conditions where Marangoni stresses maintain nearly uniform surfactant concentration (incompressible surfactant film). It was shown that for small capillary numbers, the conditions for incompressibility of the surfactant film are usually satisfied. Incompressible films may also arise in other macromolecular systems, such as lipid bilayers.

The general one-particle solution was obtained using a decomposition of the velocity field into surface-irrotational and surface-solenoidal components. Pairwise hydrodynamic mobility functions were calculated from the one-particle solution for equal-size surfactant-covered bubbles.

As the result of Marangoni stresses, the radial mobilities for drops covered with non-

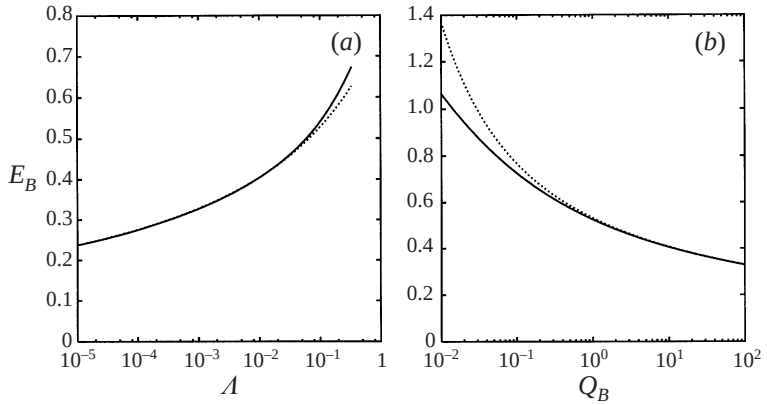

FIGURE 13. Collision efficiencies for equal-size surfactant-covered bubbles in Brownian motion: (*a*) versus surfactant diffusion parameter (without van der Waals attraction), (*b*) versus van der Waals force parameter $Q_B = kT/A_H$ (without surfactant diffusion); asymptotic formula (5.21) (dotted curves).

diffusing surfactant are the same as for rigid spheres with stick boundary conditions. In the presence of surfactant diffusion, a slip-stick boundary condition applies for axisymmetric motion.

The radial mobilities for bubbles covered with diffusing surfactant are the same as for rigid spheres with Maxwell slip. For near-contact motion, two terms in a lubrication expansion were derived. The solution is uniformly valid in the surface diffusion (Maxwell slip) parameter. The lubrication analysis applies also to moderate-viscosity-ratio drops with $\hat{\eta} \ll \Lambda^{-1/2}$.

The transverse mobilities of surfactant-covered drops are distinct from the mobilities of rigid spheres and drops with clean interfaces. In contrast to rigid spheres, surfactant-covered drops slide past each other at contact.

Collision efficiencies were calculated for equal-size surfactant-covered bubbles in straining flow, shear flow, and in Brownian motion. In the absence of surfactant diffusion and van der Waals attraction, collision efficiencies vanish because the rigid-particle-like lubrication resistance prevents contact. In shear flow, collisional efficiencies vanish for surfactant diffusion parameters smaller than a finite critical value Λ_0; in straining flow and in Brownian motion $\Lambda_0 = 0$. In all cases, finite collision efficiencies are obtained for non-zero van der Waals attraction. Asymptotic formulae for collision efficiencies in the limit of weak surfactant diffusion and weak van der Waals attraction were derived. Our asymptotic analysis may be applied to problems with other short-range lubrication cutoff mechanisms (e.g. high-viscosity drops with clean interfaces, rigid spheres with Maxwell slip) and in other flows.

Following Cichocki *et al.* (1994), our one-particle solution and lubrication results can be used to describe many-particle hydrodynamic interactions between bubbles covered with an incompressible film of diffusing surfactant.

The analysis presented herein can be extended to include surface viscous stresses. By incompressibility, the surface-dilatational viscosity is unimportant. However, the surface-solenoidal component of the flow is affected by the surface-shear viscosity. At high surfactant concentrations, surface viscous stresses may become significant. Recently, we incorporated the effects of surface viscosity in an analysis of flow in the presence of a plane surfactant-covered interface (Bławzdziewicz *et al.* 1999).

The effects of surfactant adsorption–desorption can also be incorporated within

the framework of incompressible surfactant films. Kinetically controlled adsorption is incorporated by replacing boundary condition (2.18) with

$$\nabla_s \cdot \left[\boldsymbol{w} + (\lambda a/\eta)\nabla_s\sigma\right] = \alpha\Delta\sigma, \tag{6.1}$$

where $\Delta\sigma$ is the surface tension perturbation resulting from the flow and α is an adsorption rate parameter.

Surfactant compressibility introduces nonlinearity because of the coupling between fluid velocity and surfactant concentration at the interface. For $Ma \gg 1$, drop dynamics can be analysed using a regular perturbation about the incompressible limit (Vlahovska, Bławzdziewicz & Loewenberg 1998). By a lubrication analysis, we recently determined the critical Marangoni number below which surfactant-covered drops in axisymmetric near-contact motion coalescence rapidly (Cristini *et al.* 1998).

This work was supported by NSF grant CTS-9624615, NASA grant NAG3-1935, and a grant from The Whitaker Foundation.

Appendix A. Uniqueness

The uniqueness of Stokes flow with boundary conditions (2.13)–(2.15), (2.18), corresponding to an incompressible surfactant film, is shown by considering the velocity field $\boldsymbol{v} = \boldsymbol{v}_1 - \boldsymbol{v}_2$, where $\boldsymbol{v}_1$, $\boldsymbol{v}_2$ are two Stokes flows that satisfy the boundary conditions. The energy dissipation rate generated by $\boldsymbol{v}$ is

$$E = \int_V \mathrm{d}V\ \mathbf{e} : \boldsymbol{\tau}, \tag{A 1}$$

where $\mathbf{e}$ is the strain rate and $\boldsymbol{\tau}$ is the stress tensor corresponding to $\boldsymbol{v}$. Using the divergence theorem and Stokes equations (Kim & Karrila 1991) , E is transformed:

$$E = \int_S \mathrm{d}S\ \boldsymbol{v}_s \cdot [\boldsymbol{t}_- - \boldsymbol{t}_+], \tag{A 2}$$

where $\boldsymbol{v}_s$ is the tangential component of $\boldsymbol{v}$ and $\boldsymbol{t}_\pm$ is the viscous tangential traction on the interface. Using boundary condition (2.15), we obtain

$$\begin{aligned} E &= \int_S \mathrm{d}S\ \boldsymbol{v}_s \cdot \nabla_s\sigma \\ &= -\int_S \mathrm{d}S\ \sigma\nabla_s \cdot \left(\boldsymbol{v}_s + \lambda a\eta^{-1}\nabla_s\sigma\right) - \lambda a\eta^{-1}\int_S \mathrm{d}S\ (\nabla_s\sigma)^2, \end{aligned} \tag{A 3}$$

where the first term on the right-hand side has been integrated by parts. This term vanishes by (2.18) and the second term vanishes because $E \geqslant 0$ and $\lambda a\eta^{-1} \geqslant 0$; therefore, $E = 0$. It follows that $\boldsymbol{v}_1$ and $\boldsymbol{v}_2$ are identical; thus, boundary value problem (2.12)–(2.15), (2.18) has a unique solution.

Appendix B. Decomposition of a surface vector field

We prove the existence and uniqueness of decomposition (3.1)–(3.5) for a closed simply connected surface S. On a surface with different topology the decomposition exists and is unique if supplemented with appropriate additional conditions.

A vector field normal to S automatically satisfies (3.2); we therefore consider a tangential vector field $\boldsymbol{p}$. Here, we obtain (3.1)–(3.5) in terms of intrinsic coordinates

on S. The decomposition (3.1)–(3.3) is expressed in the notation of Aris (1965):

$$p_\alpha = q_\alpha + s_\alpha, \tag{B 1}$$

$$\varepsilon^{\alpha\beta} q_{\beta,\alpha} = 0, \tag{B 2}$$

$$s^\alpha_{,\alpha} = 0, \tag{B 3}$$

where q_α is surface irrotational and s_α is surface solenoidal. Subscripts (superscripts) denote covariant (contravariant) surface components; the subscripts after a comma denote covariant differentiation. The absolute contravariant permutation tensor is $\varepsilon^{\alpha\beta}$. Relations (3.4)–(3.5) become

$$q_\alpha = \phi_{,\alpha} \tag{B 4}$$

$$s^\alpha = -\varepsilon^{\alpha\beta}\chi_{,\beta}. \tag{B 5}$$

In order to construct the fields q_α and s_α we insert (B 4)–(B 5) into (B 1) and calculate the surface curl and surface divergence of p_α. As a result, surface Poisson equations for χ and ϕ are obtained:

$$a^{\alpha\beta}\chi_{,\alpha\beta} = -\varepsilon^{\alpha\beta} p_{\beta,\alpha} \tag{B 6}$$

$$a^{\alpha\beta}\phi_{,\alpha\beta} = p^\alpha_{,\alpha} \tag{B 7}$$

where $a^{\alpha\beta}$ is the metric tensor. The integrals over S of the right-hand sides of (B 6) and (B 7) vanish, as required for existence. On a closed surface, the solution of the surface Poisson equation exists and is unique to within an additive constant. Thus, components (B 4) and (B 5) of vector field p_α exist and are unique. The difference vector

$$\delta p_\alpha = p_\alpha - q_\alpha - s_\alpha \tag{B 8}$$

satisfies

$$\varepsilon^{\alpha\beta}\delta p_{\beta,\alpha} = 0, \qquad \delta p^\alpha_{,\alpha} = 0, \tag{B 9}$$

which implies that $\delta p_\alpha = 0$; therefore decomposition (B 1) is unique.

Appendix C. One-drop solution

In this Appendix, we derive an explicit solution of Stokes equations for a spherical drop (radius a) covered with an incompressible film of diffusing surfactant. The drop is centred at $\boldsymbol{r} = 0$ and is subjected to an arbitrary incident flow $\boldsymbol{w}_0(\boldsymbol{r})$. We consider a non-translating drop (the translating drop solution is obtained by Galilean transformation).

The boundary value problem (2.12)–(2.15), (2.18) can be solved by expanding the velocity field into a complete set of solutions of the Stokes equations. We use the basic solutions defined by Felderhof and collaborators (e.g. Cichocki *et al.* 1988):

$$\boldsymbol{v}^{\pm}_{lm\sigma}(\boldsymbol{r}) = V^{\pm}_{\sigma 0}(l;r)\hat{\boldsymbol{A}}_{lm}(\boldsymbol{n}) + V^{\pm}_{\sigma 2}(l;r)\hat{\boldsymbol{B}}_{lm}(\boldsymbol{n}), \quad \sigma = 0, 2, \tag{C 1}$$

$$\boldsymbol{v}^{\pm}_{lm\sigma}(\boldsymbol{r}) = V^{\pm}_{\sigma 1}(l;r)\hat{\boldsymbol{C}}_{lm}(\boldsymbol{n}), \quad \sigma = 1, \tag{C 2}$$

where $\boldsymbol{n} = \boldsymbol{r}/r$, $l = 1, 2, \ldots$, and $m = -l, \ldots, l$. The vector spherical harmonics

$$\hat{\boldsymbol{A}}_{lm}(\boldsymbol{n}) = r^{-l+1}\nabla[r^l \hat{Y}_{lm}(\boldsymbol{n})], \qquad \hat{\boldsymbol{B}}_{lm}(\boldsymbol{n}) = r^{l+2}\nabla[r^{-(l+1)}\hat{Y}_{lm}(\boldsymbol{n})], \tag{C 3}$$

and

$$\hat{\boldsymbol{C}}_{lm}(\boldsymbol{n}) = -\boldsymbol{r} \times \nabla_s \hat{Y}_{lm}(\boldsymbol{n}), \tag{C 4}$$

with unnormalized scalar spherical harmonics

$$\hat{Y}_{lm}(\boldsymbol{n}) = (-1)^m P_l^m(\cos\theta)\mathrm{e}^{\mathrm{i}m\phi}, \tag{C 5}$$

are identical to the vector harmonics $\boldsymbol{Y}_{ll-1m}$, $\boldsymbol{Y}_{ll+1m}$, and $\boldsymbol{Y}_{llm}$ defined by Edmonds (1960), except for a different normalization. The parity of $\hat{\boldsymbol{A}}_{lm}$ and $\hat{\boldsymbol{B}}_{lm}$ is $(-1)^l$ and the parity of $\hat{\boldsymbol{C}}_{lm}$ is $(-1)^{l+1}$.

According to (C 3) and (C 4), $\hat{\boldsymbol{A}}_{lm}$ and $\hat{\boldsymbol{B}}_{lm}$ are surface irrotational and $\hat{\boldsymbol{C}}_{lm}$ are surface solenoidal. Thus, flow fields $\boldsymbol{v}^{\pm}_{lm\sigma}(\boldsymbol{r})$ are surface irrotational for $\sigma = 0, 2$ and surface solenoidal for $\sigma = 1$.

The flow fields $\boldsymbol{v}^{+}_{lm\sigma}$ are regular at $r = 0$ and the fields $\boldsymbol{v}^{-}_{lm\sigma}$ are regular at $r \to \infty$. Explicit expressions for the functions $V^{\pm}_{\sigma\sigma'}(l;r)$ are (Cichocki *et al.* 1988)

$$V^{+}_{00}(l;r) = r^{l-1}, \qquad V^{+}_{02}(l;r) = 0, \tag{C 6}$$

$$V^{+}_{20}(l;r) = \frac{(l+1)(2l+3)}{2l} r^{l+1}, \qquad V^{+}_{22}(l;r) = r^{l+1}, \tag{C 7}$$

$$V^{+}_{11}(l;r) = \mathrm{i}r^{l} \tag{C 8}$$

and

$$V^{-}_{00}(l;r) = \frac{l+1}{l(2l-1)(2l+1)^2} r^{-l}, \qquad V^{-}_{02}(l;r) = -\frac{1}{2(2l+1)^2} r^{-l}, \tag{C 9}$$

$$V^{-}_{20}(l;r) = 0, \qquad V^{-}_{22}(l;r) = \frac{l}{(l+1)(2l+1)^2(2l+3)} r^{-(l+2)}, \tag{C 10}$$

$$V^{-}_{11}(l;r) = \frac{\mathrm{i}}{l(l+1)(2l+2)} r^{-(l+1)}. \tag{C 11}$$

Only $\boldsymbol{v}^{+}_{lm2}(\boldsymbol{r})$ and $\boldsymbol{v}^{-}_{lm0}(\boldsymbol{r})$ are associated with non-zero pressure fields:

$$p^{+}_{lm2}(\boldsymbol{r}) = \eta \frac{(l+1)(2l+1)(2l+3)}{l} r^{l} \hat{Y}_{lm}(\boldsymbol{n}), \tag{C 12}$$

$$p^{-}_{lm0}(\boldsymbol{r}) = \eta \frac{1}{2l+1} r^{-(l+1)} \hat{Y}_{lm}(\boldsymbol{n}). \tag{C 13}$$

The total velocity field $\boldsymbol{w}(\boldsymbol{r})$ is decomposed into the incident and scattered fields:

$$\boldsymbol{w}(\boldsymbol{r}) = \boldsymbol{w}_0(\boldsymbol{r}) + \boldsymbol{w}_1(\boldsymbol{r}), \tag{C 14}$$

where $\boldsymbol{w}_1(\boldsymbol{r}) = 0$ for $r \to \infty$. The flow fields are expanded into spherical components (C 1)–(C 2):

$$\boldsymbol{w}_0(\boldsymbol{r}) = \sum_{lm\sigma} c^{+}_{lm\sigma} \boldsymbol{v}^{+}_{lm\sigma}(\boldsymbol{r}), \tag{C 15}$$

$$\boldsymbol{w}_1(\boldsymbol{r}) = \sum_{lm\sigma} c^{-}_{lm\sigma} \boldsymbol{v}^{-}_{lm\sigma}(\boldsymbol{r}), \quad r \geqslant a, \tag{C 16}$$

$$\boldsymbol{w}_1(\boldsymbol{r}) = \sum_{lm\sigma} \tilde{c}^{+}_{lm\sigma} \boldsymbol{v}^{+}_{lm\sigma}(\boldsymbol{r}), \quad r \leqslant a. \tag{C 17}$$

The amplitudes of the incident and reflected spherical components of the flow are linearly related:

$$c^{-}_{lm\sigma} = \sum_{l'm'\sigma'} X(lm\sigma, l'm'\sigma') c^{+}_{l'm'\sigma'}, \tag{C 18}$$

where $X(lm\sigma, l'm'\sigma')$ is the scattering matrix characterizing the response of the system to the incident flow. Solutions with different parity or different l do not couple; thus,

$$X(lm\sigma, l'm'\sigma') = \delta_{ll'}\delta_{mm'}\overline{X}^{l}_{\sigma\sigma'}, \tag{C 19}$$

where

$$\overline{X}^{l}_{\sigma\sigma'} = \begin{bmatrix} \overline{X}^{l}_{00} & 0 & \overline{X}^{l}_{02} \\ 0 & \overline{X}^{l}_{11} & 0 \\ \overline{X}^{l}_{02} & 0 & \overline{X}^{l}_{22} \end{bmatrix} \tag{C 20}$$

(Schmitz & Felderhof 1978; Cichocki *et al.* 1988).

Matrix elements X^{l}_{11} describe the coupling between the surface-solenoidal components of the incident and scattered flow fields. According to (3.9), surface-solenoidal flows are unaffected by surfactant. The X^{l}_{11} are therefore the same as for a drop with a clean interface; expressions are given by Cichocki *et al.* (1988).

Matrix elements X^{l}_{00}, X^{l}_{02}, and X^{l}_{22} describe coupling between surface-irrotational components of the incident and scattered flow fields. Surface-irrotational flows satisfy the stick boundary condition in the absence of surfactant diffusion and the slip-stick boundary condition (3.11) for bubbles covered with diffusing surfactant. Elements of the scattering matrix (C 20) are known for both cases (Cichocki *et al.* 1988).

For viscous drops covered with an incompressible film of diffusing surfactant, surface-irrotational flows satisfy a slip-stick boundary condition (3.8), (3.10). The solution of the corresponding boundary value problem is derived below.

For this purpose, we introduce matrix notation in the subspace $\sigma = 0, 2$. Accordingly, $\underset{\sim}{x}$ denotes an array with elements x_σ and $\underset{\approx}{Y}$ denotes a matrix with elements $Y_{\sigma\sigma'}$, where $\sigma, \sigma' = 0, 2$. Thus, $\underset{\sim}{\boldsymbol{v}}^{\pm}_{lm}(\boldsymbol{r})$ has elements $\boldsymbol{v}^{\pm}_{lm\sigma}(\boldsymbol{r})$ and $\underset{\approx}{V}^{\pm}(l;r)$ has elements $V^{\pm}_{\sigma\sigma'}(l;r)$.

Two arrays of vector spherical harmonics are introduced:

$$\underset{\sim}{\boldsymbol{h}}^{A}_{lm}(\boldsymbol{n}) = \begin{bmatrix} \hat{\boldsymbol{A}}_{lm}(\boldsymbol{n}) \\ \hat{\boldsymbol{B}}_{lm}(\boldsymbol{n}) \end{bmatrix}, \qquad \underset{\sim}{\boldsymbol{h}}^{S}_{lm}(\boldsymbol{n}) = \begin{bmatrix} \hat{\boldsymbol{R}}_{lm}(\boldsymbol{n}) \\ \hat{\boldsymbol{S}}_{lm}(\boldsymbol{n}) \end{bmatrix}, \tag{C 21}$$

where $\hat{\boldsymbol{A}}_{lm}$ and $\hat{\boldsymbol{B}}_{lm}$ are defined by (C 3) and

$$\hat{\boldsymbol{S}}_{lm} = r\nabla_s \hat{Y}_{lm}, \qquad \hat{\boldsymbol{R}}_{lm} = \hat{Y}_{lm}\boldsymbol{n}. \tag{C 22}$$

The relation between the matrices $\underset{\sim}{\boldsymbol{h}}^{S}_{lm}$ and $\underset{\sim}{\boldsymbol{h}}^{A}_{lm}$ is

$$\underset{\sim}{\boldsymbol{h}}^{A}_{lm} = \underset{\approx}{H}_{lm}\underset{\sim}{\boldsymbol{h}}^{S}_{lm}, \tag{C 23}$$

where

$$\underset{\approx}{H}_{lm} = \begin{bmatrix} l & 1 \\ -(l+1) & 1 \end{bmatrix}. \tag{C 24}$$

Hereafter, we omit indices l and m since the problem is diagonal.

A transformed set of basic solutions

$$\underset{\sim}{\boldsymbol{u}}^{\pm}(\boldsymbol{r}) = \underset{\approx}{\Psi}^{\pm}\underset{\sim}{\boldsymbol{v}}^{\pm}(\boldsymbol{r}), \tag{C 25}$$

where

$$\underset{\approx}{\Psi}^{\pm} = \left[\underset{\approx}{V}^{\pm}(a)\underset{\approx}{H}\right]^{-1}, \tag{C 26}$$

is used to construct solutions that satisfy boundary condition (2.14). Expressions

$$\underset{\sim}{\boldsymbol{v}}^{\pm}(\boldsymbol{r}) = \underset{\approx}{V}^{\pm}(r)\underset{\sim}{\boldsymbol{h}}^{A}(\boldsymbol{n}) \tag{C 27}$$

and (C 23) indicate that

$$\underset{\sim}{\boldsymbol{u}}^{\pm}(a\boldsymbol{n}) = \underset{\sim}{\boldsymbol{h}}^{S}(\boldsymbol{n}); \tag{C 28}$$

thus,

$$\boldsymbol{n}\cdot\boldsymbol{u}_0^{\pm} \neq 0, \qquad \boldsymbol{n}\cdot\boldsymbol{u}_2^{\pm} = 0 \tag{C 29}$$

at $r = a$.

By symmetry, tangential surface tractions associated with $\boldsymbol{u}_\sigma^{\pm}$ have the form

$$\boldsymbol{t}_{u,\sigma}^{\pm} = (\eta/a) t_{u,\sigma}^{\pm} \hat{\boldsymbol{S}}_{lm}, \qquad \sigma = 0, 2. \tag{C 30}$$

The coefficients $t_{u,\sigma}^{\pm}$ can be evaluated:

$$\underset{\sim}{t}_u^{+} = \begin{bmatrix} -3/l \\ 2l+1 \end{bmatrix}, \tag{C 31}$$

$$\underset{\sim}{t}_u^{-} = \begin{bmatrix} 3/(l+1) \\ -(2l+1) \end{bmatrix}, \tag{C 32}$$

According to (C 22), tractions (C 30) are surface gradients of scalar functions.

The most general solution of the Stokes equations that tends to the incident field

$$\boldsymbol{w}_0(\boldsymbol{r}) = \underset{\sim}{\varsigma}^{+} \cdot \underset{\sim}{\boldsymbol{y}}^{+}(\boldsymbol{r}) \tag{C 33}$$

at large r and satisfies boundary conditions (2.13)–(2.14) is

$$\boldsymbol{w}(\boldsymbol{r}) = \underset{\sim}{\varsigma}^{+} \cdot \left[\underset{\approx}{\Psi}^{+}\right]^{-1} \left[\underset{\sim}{\boldsymbol{u}}^{+}(\boldsymbol{r}) - \underset{\sim}{\boldsymbol{u}}^{-}(\boldsymbol{r})\right] + \alpha \boldsymbol{u}_2^{-}(\boldsymbol{r}), \quad r \geqslant a, \tag{C 34}$$

$$\boldsymbol{w}(\boldsymbol{r}) = \alpha \boldsymbol{u}_2^{+}(\boldsymbol{r}), \quad r \leqslant a, \tag{C 35}$$

where α is determined by the boundary condition for surface tractions. The interfacial tangential tractions associated with this solution are

$$\boldsymbol{t}_{\pm}(\boldsymbol{n}) = (\eta/a) t_{\pm}^{w} \hat{\boldsymbol{S}}_{lm}(\boldsymbol{n}), \tag{C 36}$$

where

$$t_{+}^{w} = \underset{\sim}{\varsigma}^{+} \cdot \left[\underset{\approx}{\Psi}^{+}\right]^{-1} \left(\underset{\sim}{t}_u^{+} - \underset{\sim}{t}_u^{-}\right) + \alpha t_{u,2}^{-} \tag{C 37}$$

and

$$t_{-}^{w} = \alpha t_{u,2}^{+}, \tag{C 38}$$

as indicated by (C 30).

Boundary condition (2.15) implies that

$$\nabla\sigma(\boldsymbol{n}) = -(\eta/a)\left[t_{+}^{w} - \hat{\eta} t_{-}^{w}\right] \hat{\boldsymbol{S}}_{lm}(\boldsymbol{n}). \tag{C 39}$$

Using (3.10), (C 28) and (C 35), the result is reduced to

$$\alpha - \lambda\left[t_{+}^{w} - \hat{\eta} t_{-}^{w}\right] = 0. \tag{C 40}$$

From (C 37), (C 38) and (C 40) we obtain

$$\alpha = \frac{\underset{\sim}{\varsigma}^{+} \cdot \left[\underset{\approx}{\Psi}^{+}\right]^{-1} \left(\underset{\sim}{t}_u^{+} - \underset{\sim}{t}_u^{-}\right)}{\lambda^{-1} + \hat{\eta} t_{u,2}^{+} - t_{u,2}^{-}}. \tag{C 41}$$

Inserting the result into (C 34) and transforming back to the representation in terms of the basic solutions $\underset{\sim}{\boldsymbol{y}}^{\pm}$ yields

$$\boldsymbol{w}(\boldsymbol{r}) = \underset{\sim}{\varsigma}^{+} \cdot \left[\underset{\sim}{\boldsymbol{y}}^{+}(\boldsymbol{r}) + \underset{\approx}{X}\underset{\sim}{\boldsymbol{y}}^{-}(\boldsymbol{r})\right], \tag{C 42}$$

where

$$\overline{\underset{\approx}{X}} = \left[\underset{\approx}{\Psi}^{+}\right]^{-1}\left[\underset{\approx}{\hat{I}} + \underset{\approx}{\Gamma}\right]\underset{\approx}{\Psi}^{-} \tag{C 43}$$

with

$$\Gamma_{ij} = \frac{\left(t^{+}_{u,i} - t^{-}_{u,i}\right)\delta_{j2}}{\lambda^{-1} + \hat{\eta}t^{+}_{u,2} - t^{-}_{u,2}}. \tag{C 44}$$

By comparing (C 18)–(C 19) with (C 42) and using symmetry of the matrix $\overline{X}$, we conclude that $\overline{\underset{\approx}{X}}$ is identical to the submatrix $\left[\overline{X}_{\sigma\sigma'}\right]_{\sigma,\sigma'=0,2}$.

Evaluating (C 43)–(C 44) yields

$$\overline{X}^{l}_{\sigma\sigma'} = (2l+1)\begin{bmatrix} \dfrac{2l(2l-1)}{l+1}A_{l0} & 0 & (2l-1)(2l+1)A_{l2} \\ 0 & l(l+1)A_{l1} & 0 \\ (2l-1)(2l+1)A_{l2} & 0 & \dfrac{(l+1)(2l+1)^2(2l+3)}{2l}B_{l2} \end{bmatrix}, \tag{C 45}$$

with

$$\begin{aligned} A_{l0} &= \frac{2l+1}{2}\frac{\nu(1-\Lambda)+(2l+1)\Lambda}{\nu[1+2(l-1)\Lambda]+(2l+1)\Lambda}a^{2l-1}, \\ A_{l2} &= \frac{2l+3}{2}\frac{\nu(1-3\Lambda)+(2l+1)\Lambda}{\nu[1+2(l-1)\Lambda]+(2l+1)\Lambda}a^{2l+1}, \\ B_{l2} &= \frac{2l+1}{2}\frac{\nu(1-5\Lambda)+(2l+1)\Lambda}{\nu[1+2(l-1)\Lambda]+(2l+1)\Lambda}a^{2l+3}, \end{aligned} \tag{C 46}$$

where $\nu = 1/\hat{\eta}$ and Λ is defined by (4.4). The results for rigid spheres are recovered for $\Lambda \to 0$ or $\nu \to 0$, the results for the slip-stick boundary condition (3.11) are recovered for $\nu \to \infty$, and the results for drops with clean interfaces are recovered for $\Lambda \to \frac{1}{3}$ (cf. Cichocki *et al.* 1988).

For completeness, we also give the coefficients for the surface-solenoidal solutions

$$A_{l1} = \frac{(l-1)(1-\nu)}{l-1+(l+2)\nu}a^{2l+1}, \tag{C 47}$$

which are the same as for drops with clean interfaces (Cichocki *et al.* 1988) .

The translational friction coefficient for an isolated drop is given by

$$\zeta_1 = 4\pi\eta A_{10}, \tag{C 48}$$

which yields

$$\zeta_1 = 6\pi\eta a\frac{\nu(1-\Lambda)+3\Lambda}{\nu+3\Lambda} \tag{C 49}$$

for a surfactant-covered drop.

Appendix D. Evaluation of pair mobilities

We evaluated mobility functions $A(R)$, $B(R)$, $G(R)$, and $H(R)$ for bubbles covered with an incompressible film of diffusing surfactant. The mobility functions were obtained from the one-particle scattering matrix (C 45) using the multiple scattering

algorithm developed by Cichocki *et al.* (1988). Accordingly, a pair mobility function $\mu(R)$ is obtained as a series

$$\mu(R) = \sum_{l=0}^{\infty} \mu^{(l)} R^{-l}, \tag{D 1}$$

where the expansion coefficients $\mu^{(l)}$ are calculated numerically.

For $\lambda \neq 0$ the expansion coefficients of mobility functions A and G have the asymptotic behaviour

$$\mu^{(l)} = \frac{C}{l(\ln l)^2}\left[1 + O\left(\frac{1}{\ln l}\right)\right] \tag{D 2}$$

for large l, where C is a constant. As shown by Cichocki & Felderhof (1988), this corresponds to the logarithmic behaviour

$$\mu(R) = C' + \frac{C}{\ln \epsilon^{-1}} + O\left(\frac{1}{\ln \epsilon^{-1}}\right)^2 \tag{D 3}$$

of the mobility functions for small gap widths $\epsilon \ll 1$. The logarithmic behaviour of A and G is consistent with the lubrication analysis presented in § 4.3. Mobility functions B and H are analytic for $\epsilon \to 0$ thus, expansion (D 1) converges rapidly.

The mobility functions A, B, G, and H presented in figures 1–4 were obtained from the series (D 1) with up to 1400 numerically evaluated coefficients. For A and G, the series was extrapolated using a low-order polynomial in $1/\ln l$ to approximate $l(\ln l)^2\mu^{(l)}$.

Appendix E. Lubrication analysis

In this Appendix, the method of Jeffrey (1982) and Kim & Karrila (1991) is used to analyse the near-contact axisymmetric motion of two equal-size bubbles covered with an incompressible film of diffusing surfactant.

We use a cylindrical coordinate system with radial coordinate ρ and axial coordinate z along the line of centres. The symmetry plane is at $z = 0$ and $\hat{\boldsymbol{e}}_z$ is a unit vector in the z-direction. The bubbles have centres at $z_i = \mp(1 + \frac{1}{2}\epsilon)a$ and velocities $\boldsymbol{U}_i = \pm\frac{1}{2}U_{12}\hat{\boldsymbol{e}}_z$, where the upper sign corresponds to $i = 1$ and the lower sign to $i = 2$.

Fluid velocity at the interface $z = z_{si}(\rho)$ of drop i is

$$\boldsymbol{w}(\rho, z_{si}(\rho)) = \pm\tfrac{1}{2}U_{12}\hat{\boldsymbol{e}}_z + w_t\hat{\boldsymbol{e}}_t, \tag{E 1}$$

where $\hat{\boldsymbol{e}}_t$ is the unit vector tangent to the interface in the meridian plane. By symmetry, the flow is surface irrotational. Thus, the slip-stick boundary condition (3.11) applies:

$$w_t = (\lambda a/\eta)\boldsymbol{t}_+, \tag{E 2}$$

where $\boldsymbol{t}_+ = t_+\hat{\boldsymbol{e}}_t$ is the viscous tangential traction on the interface.

The radial and axial velocity components are obtained from the stream function ψ:

$$w_\rho = U_{12}\frac{1}{\rho}\frac{\partial\psi}{\partial z}, \tag{E 3}$$

$$w_z = -U_{12}\frac{1}{\rho}\frac{\partial\psi}{\partial\rho}, \tag{E 4}$$

where

$$\mathrm{E}^4\psi = 0 \tag{E 5}$$

and

$$\mathrm{E}^2 = \frac{\partial^2}{\partial z^2} + \frac{\partial^2}{\partial r^2} - \frac{1}{r}\frac{\partial}{\partial r}. \tag{E 6}$$

Boundary conditions for the stream function are given by (E 2) and

$$\psi(\rho, z_{si}(\rho)) = \mp\tfrac{1}{4}\rho^2, \quad i = 1, 2, \tag{E 7}$$

which follows from (E 1).

We transform to lubrication coordinates:

$$\bar{\rho} = \epsilon^{-1/2}\frac{\rho}{a}, \quad \bar{z} = \epsilon^{-1}\frac{z}{a} \tag{E 8}$$

in which the sphere surfaces are

$$\bar{z}_{si} = \mp(\tfrac{1}{2} + \tfrac{1}{2}\bar{\rho}^2 + \tfrac{1}{8}\epsilon\bar{\rho}^4) + O(\epsilon^2). \tag{E 9}$$

We also rescale the slip parameter:

$$\bar{\lambda} = \lambda/\epsilon. \tag{E 10}$$

The expansion

$$\psi = a^2\epsilon\left[\psi_0 + \epsilon\psi_1 + O(\epsilon^2)\right] \tag{E 11}$$

inserted into the rescaled (E 5) yields

$$\frac{\partial^4\psi_0}{\partial\bar{z}^4} = 0, \qquad \frac{\partial^4\psi_1}{\partial\bar{z}^4} = -2\hat{\mathscr{R}}\frac{\partial^2\psi_0}{\partial\bar{z}^2}, \tag{E 12}$$

where

$$\hat{\mathscr{R}} = \frac{\partial^2}{\partial\bar{\rho}^2} - \frac{1}{\bar{\rho}}\frac{\partial}{\partial\bar{\rho}}. \tag{E 13}$$

The solution of (E 12) has the form

$$\psi_0 = A_{01}(\bar{\rho})\bar{z} + A_{03}(\bar{\rho})\bar{z}^3, \tag{E 14}$$

$$\psi_1 = A_{11}(\bar{\rho})\bar{z} + A_{13}(\bar{\rho})\bar{z}^3 + A_{15}(\bar{\rho})\bar{z}^5, \tag{E 15}$$

where even terms vanish by symmetry and

$$A_{15}(\bar{\rho}) = -\tfrac{1}{10}\hat{\mathscr{R}}A_{03}(\bar{\rho}). \tag{E 16}$$

The coefficients A_{ij} with $i = 0, 1$ and $j = 1, 3$ are determined by boundary conditions (E 2) and (E 7). At the leading order in ϵ:

$$\frac{1+\bar{\rho}^2}{2}A_{01}(\bar{\rho}) + \left(\frac{1+\bar{\rho}^2}{2}\right)^3 A_{03}(\bar{\rho}) = \frac{\bar{\rho}^2}{4}, \tag{E 17}$$

$$A_{01}(\bar{\rho}) + \tfrac{3}{4}\left(1+\bar{\rho}^2\right)\left(1+4\bar{\lambda}+\bar{\rho}^2\right)A_{03}(\bar{\rho}) = 0. \tag{E 18}$$

At the next order, we obtain

$$A_{11} + \tfrac{1}{4}\left(1+\bar{\rho}^2\right)^2 A_{13} = -Q_1(\bar{\rho}), \tag{E 19}$$

$$A_{11} + \tfrac{3}{4}\left(1+\bar{\rho}^2\right)\left(1+4\bar{\lambda}+\bar{\rho}^2\right)A_{13} = -Q_2(\bar{\rho}), \tag{E 20}$$

where

$$Q_1 = \frac{\bar{\rho}^4}{4(1+\bar{\rho}^2)}A_{01} + \tfrac{3}{16}\bar{\rho}^4(1+\bar{\rho}^2)A_{03} + \tfrac{1}{16}(1+\bar{\rho}^2)^4 A_{15} \tag{E 21}$$

and

$$Q_2 = \left(2\bar{\lambda} - \frac{\bar{\rho}^2}{2}\right) A_{01} - \frac{1}{2\bar{\rho}}\left[\bar{\rho}^2 + \bar{\rho}^4 + \bar{\lambda}\left(-1 + 7\bar{\rho}^2\right)\right] A'_{01} - \tfrac{1}{2}\bar{\lambda}\left(1 + \bar{\rho}^2\right) A''_{01}$$
$$-\tfrac{3}{8}\left[\bar{\rho}^2 + \bar{\rho}^4 + 2\bar{\lambda}\left(-2 + 4\bar{\rho}^2 + 5\bar{\rho}^4\right)\right] A_{03}$$
$$-\frac{1}{8\bar{\rho}}\left(1 + \bar{\rho}^2\right)^2\left[\bar{\rho}^2 + \bar{\rho}^4 + \bar{\lambda}\left(-1 + 23\bar{\rho}^2\right)\right] A'_{03} - \tfrac{1}{8}\bar{\lambda}\left(1 + \bar{\rho}^2\right)^3 A''_{03}$$
$$+\tfrac{5}{16}\bar{\rho}\left(1 + \bar{\rho}^2\right)^3\left(1 + 8\bar{\lambda} + \bar{\rho}^2\right) A_{15} + \tfrac{1}{2}\rho^2, \tag{E 22}$$

with prime denoting the derivative with respect to $\bar{\rho}$. Equations (E 17)–(E 18) and (E 19)–(E 20) with A_{15} given by (E 16) are solved consecutively.

The hydrodynamic force on bubble i is

$$\frac{F_{zi}}{\pi\eta a U_{12}} = \int_0^\pi \rho^3 \frac{\partial}{\partial r}\frac{\mathrm{E}^2\psi}{\rho^2}\,\mathrm{d}s \tag{E 23}$$

where r is the radial spherical coordinate from the centre of the bubble, s is arc length in radians, and the integration is on the interface along an arc in the meridian plane. Transforming (E 23) into lubrication variables, inserting ψ given by (E 11) and (E 14)–(E 15) with the expansion coefficients from (E 16)–(E 22), and expanding in powers of ϵ yields the contribution to the force from the integral over the inner lubrication region:

$$\frac{F_{zi}}{\pi\eta a U_{12}} = \mp\left[\epsilon^{-1} I_0(\bar{\rho}_0) + I_1(\bar{\rho}_0)\right] + O(\epsilon), \tag{E 24}$$

where $1 \ll \bar{\rho}_0 \ll \epsilon^{-1/2}$ defines the matching region between the inner and outer regions. The error estimate was obtained for fixed $\bar{\rho}_0$. Explicit calculations yield

$$I_0 = 3\left[\frac{1}{\bar{\delta}^2}\left(1 + \bar{\delta}\right)\ln\left(1 + \bar{\delta}\right) - \frac{1}{\bar{\delta}}\right] + O(\bar{\rho}_0^{-2}), \tag{E 25}$$

$$I_1 = \frac{1}{20}\left[\frac{-17 + 20\bar{\delta} + \frac{103}{3}\bar{\delta}^2}{\bar{\delta}\left(1 + \bar{\delta}\right)} + \frac{17 + 30\bar{\delta} - 7\bar{\delta}^2}{\bar{\delta}^2}\ln\left(1 + \bar{\delta}\right) + 27\ln\bar{\rho}_0^2\right] + O(\bar{\rho}_0^{-2}), \tag{E 26}$$

where $\bar{\delta} = 6\bar{\lambda}$.

We assume that the $O(\bar{\rho}_0^{-2})$ terms in (E 25)–(E 26) are cancelled by contributions from the outer region and the $\ln\bar{\rho}_0^2$ term produces the $\ln\epsilon^{-1}$ contribution (O'Neill & Stewartson 1967; Kim & Karrila 1991). Thus, (E 24)–(E 26) yield (4.5)–(4.9).

Our analysis is for $\bar{\delta}$ fixed; thus, (E 24)–(E 26) is strictly valid only for small λ. However, the numerical results discussed in § 4.3 indicate that the modified formula (4.12) is uniformly valid for all λ.

Appendix F. Asymptotic analysis of collision efficiencies

F.1. *Axisymmetric straining flow*

F.1.1. *Weak surfactant diffusion*

To derive (5.9) we note that for small $\Lambda \equiv \epsilon^*$, the asymptotic form of integral (5.7) is

$$I_{st}(1) = \int_0^\infty f_0(\epsilon) g(\epsilon/\epsilon^*)\,\mathrm{d}\epsilon + o(1), \quad \epsilon^* \ll 1, \tag{F 1}$$

with

$$f_0(\epsilon) = \frac{1}{2+\epsilon}\frac{A_0(R) - B_0(R)}{1 - A_0(R)}, \tag{F 2}$$

where $R = 1 + \frac{1}{2}\epsilon$ and A_0, B_0 are the mobilities for $\Lambda = 0$. The leading-order correction resulting from surfactant diffusion is described by

$$g(\epsilon/\epsilon^*) = 2\epsilon\zeta_G^{(0)}, \tag{F 3}$$

where $\zeta_G^{(0)}$ is given by (4.8). The asymptotic behaviour of f_0 and g is

$$f_0(\epsilon) \approx \frac{\beta}{\epsilon} \text{ for } \epsilon \ll 1, \tag{F 4}$$

$$g(\epsilon/\epsilon^*) \approx 1 \text{ for } \epsilon \gg \epsilon^*, \tag{F 5}$$

where

$$\beta = \frac{1 - B_0(1)}{4D_0} \tag{F 6}$$

and D_0 is the mobility ratio D for $\Lambda = 0$. Integral (F 1) exists because the integrand vanishes sufficiently fast for $\epsilon \to \infty$ and the singularity $\epsilon^{-1}g(\epsilon/\epsilon^*)$ for $\epsilon \to 0$ is integrable.

Using contact values of the mobility functions for equal-size surfactant-covered bubbles, given in table 1, we obtain

$$\beta = 0.10446. \tag{F 7}$$

For small ϵ^*, $I_{st}(1)$ can be decomposed into integrals over outer and inner regions:

$$I_{st}(1) = I_1 + I_2, \tag{F 8}$$

where

$$I_1 = \int_{\epsilon_m}^{\infty} f_0(\epsilon)g(\epsilon/\epsilon^*)\,\mathrm{d}\epsilon, \tag{F 9}$$

$$I_2 = \int_0^{\epsilon_m} f_0(\epsilon)g(\epsilon/\epsilon^*)\,\mathrm{d}\epsilon, \tag{F 10}$$

with

$$\epsilon^* \ll \epsilon_m \ll 1. \tag{F 11}$$

According to (F 4)–(F 5)

$$I_1 = -\beta \ln(\epsilon_m) + C_1, \tag{F 12}$$

$$I_2 = \beta \ln(\epsilon_m/\epsilon^*) + C_2, \tag{F 13}$$

where C_1 and C_2 are constants; thus,

$$I_{st}(1) = -\beta \ln \epsilon^* + \tfrac{1}{3}\ln \Gamma_1, \tag{F 14}$$

where $\ln \Gamma_1 = 3(C_1 + C_2)$. Formula (5.9) is obtained by inserting (F 14) into (5.6).

F.1.2. *Weak van der Waals attraction*

The asymptotic behaviour of E_{st} for drops covered with non-diffusing surfactant ($\Lambda = 0$) is found by a boundary-layer analysis for interparticle potentials that have a power-law form

$$\Phi = -\alpha\epsilon^{-m}, \tag{F 15}$$

for small gaps, where α and m are constants. The relative bubble motion is described by the trajectory equation (cf. Wang *et al.* 1994)

$$\frac{\mathrm{d}\epsilon}{\mathrm{d}\theta} = \frac{-(2+\epsilon)[1-A_0(R)](3\cos^2\theta - 1) \pm \dfrac{G_0(R)}{\overline{Q}}\dfrac{\mathrm{d}\Phi}{\mathrm{d}\epsilon}}{3[1-B_0(R)]\sin\theta\cos\theta}, \tag{F 16}$$

where θ is the azimuthal angle measured from the symmetry axis of the flow and

$$\overline{Q} = \frac{\eta\dot{\gamma}a^2}{2\mu_1\alpha}. \tag{F 17}$$

The upper (lower) sign corresponds to uniaxial extensional (compressional) flow.

For $\epsilon \ll 1$ the trajectory equation simplifies to

$$\frac{\mathrm{d}\ln(\epsilon/\bar{\epsilon}^*)}{\mathrm{d}\theta} = -\frac{\mathrm{d}\ln(\sin^2\theta\cos\theta)}{3\beta\,\mathrm{d}\theta} \pm \frac{2m}{3[1-B_0(1)]\sin\theta\cos\theta}\left(\frac{\epsilon}{\bar{\epsilon}^*}\right)^{-(m+1)}, \tag{F 18}$$

where β is defined by (F 6) and

$$\bar{\epsilon}^* = \overline{Q}^{-1/(m+1)}. \tag{F 19}$$

Thus,

$$\frac{\epsilon}{\bar{\epsilon}^*} = q(\theta), \tag{F 20}$$

where q is independent of $\overline{Q}$.

For $\epsilon \gg \bar{\epsilon}^*$, the interparticle force is unimportant and the solution of (F 16) is (Wang *et al.* 1994)

$$C\mathrm{e}^{3I_{st}(R)} = \tfrac{1}{8}(2+\epsilon)^3\sin^2\theta\cos\theta, \tag{F 21}$$

where $I_{st}(R)$ is defined by (5.7) and constant C specifies the trajectory; in the matching region $\bar{\epsilon}^* \ll \epsilon \ll 1$, (F 18) yields

$$C^*\left(\frac{\epsilon}{\bar{\epsilon}^*}\right)^{-3\beta} = \sin^2\theta\cos\theta. \tag{F 22}$$

Matching (F 22) and (F 21) requires

$$C = \mathrm{e}^{-3C_1}C^*\bar{\epsilon}^{*3\beta}, \tag{F 23}$$

where the asymptotic form (F 12) has been used.

Following Zinchenko (1984), the critical parameter $\overline{C}$ is defined, such that trajectories (F 21) with $|C| > \overline{C}$ are unbounded and with $|C| < \overline{C}$ reach the collisional surface $\epsilon = 0$. The corresponding critical parameter for the solution in the inner region is denoted by $\overline{C}^*$.

The flux of colliding trajectories incoming from infinity is $\pi\dot{\gamma}\overline{C}$; thus,

$$E_{st} = \frac{\overline{C}}{\overline{C}_0}, \tag{F 24}$$

where $\overline{C}_0 = 16/(3\sqrt{3})$ is the critical parameter in the absence of van der Waals and hydrodynamic interactions. Using (F 23) and (F 24) we obtain

$$E_{st} = \Gamma'\bar{\epsilon}^{*3\beta}, \tag{F 25}$$

where

$$\Gamma' = \frac{\mathrm{e}^{-3C_1}\overline{C}^*}{C_0} \tag{F 26}$$

is independent of $\overline{Q}$ by relation (F 20).

The unretarded van der Waals potential (5.4) is described using $m = 1$ in (F 15) and the retarded potential (5.5) is described using $m = 2$. Thus, asymptotic result (5.9) is obtained with (5.10) for an unretarded and (5.11) for a fully-retarded van der Waals potential.

F.2. *Shear flow*

F.2.1. *Weak surfactant diffusion*

To find the asymptotic behaviour of $I_{sh}(1)$ for small $\Lambda \equiv \epsilon^*$, (5.14) is rewritten

$$I_{sh}(1) = -\tfrac{1}{2}\int_1^\infty w(t)\frac{\mathrm{d}}{\mathrm{d}t}\mathrm{e}^{-2I_{st}(t)}\,\mathrm{d}t, \tag{F 27}$$

where

$$w(t) = \frac{t^2 B(t)}{A(t) - B(t)}, \tag{F 28}$$

which has the limiting behaviour for $\epsilon^*, \epsilon \ll 1$

$$w_0 = \frac{B_0(1)}{1 - B_0(1)}. \tag{F 29}$$

Thus, (F 27) yields

$$I_{sh}(1) = -\tfrac{1}{2}w_0\mathrm{e}^{-2I_{st}(1)} + C' \text{ for } \epsilon^* \ll 1. \tag{F 30}$$

By numerical integration,

$$C' = 0.10621 \tag{F 31}$$

for equal-size surfactant-covered bubbles. Combining (F 14) and (F 30) gives

$$I_{sh}(1) = -\tfrac{1}{2}w_0\Gamma_1^{2/3}\epsilon^{*2\beta} + C' \text{ for } \epsilon^* \ll 1, \tag{F 32}$$

which is inserted with (5.9) into (5.12) to yield (5.17) where

$$\Gamma_2 = \Gamma_1(1 + \tfrac{1}{2}w_0)^{3/2} \tag{F 33}$$

and

$$\Lambda_0 = C'^{1/2\beta}\Gamma_2^{-1/3\beta}. \tag{F 34}$$

F.2.2. *Weak van der Waals attraction*

Here, we assume $\Lambda < \Lambda_0$; therefore, the region of finite trajectories encloses the collision surface. For weak van der Waals attraction, the particle pair distribution function g is unperturbed outside the finite-trajectory envelope Ω and thus (Batchelor & Green 1972*a*)

$$g(\epsilon) = \frac{1}{1 - A(R)}\mathrm{e}^{-3I_{st}(R)}. \tag{F 35}$$

From (5.1),

$$E_{sh} = \tfrac{3}{32}a^{-2}\int_\Omega g(\epsilon)(\boldsymbol{u}\cdot\boldsymbol{n})\,\mathrm{d}S, \tag{F 36}$$

where

$$\boldsymbol{u} = \tfrac{1}{2}Q^{-1}G(R)f(\epsilon)\hat{\boldsymbol{r}}_{12} \tag{F 37}$$

is the drift velocity, normalized by $\dot{\gamma}a$, and

$$f = -\frac{1}{A_H}\frac{\mathrm{d}\Phi}{\mathrm{d}\epsilon} \tag{F 38}$$

is the dimensionless van der Waals force. Thus (5.18) is obtained with

$$\Gamma_3 = \int_\Omega g(\epsilon)G(R)f(\epsilon)(\hat{\boldsymbol{r}}_{12}\cdot\boldsymbol{n})\,\mathrm{d}S. \tag{F 39}$$

An estimate for Γ_3 is obtained by inserting $\epsilon \approx \epsilon_{\min}$ into (F 39), where $\epsilon_{\min}$ is the minimum thickness of the closed trajectory region. For drops covered with non-diffusing surfactant, (F 35) yields

$$g(\epsilon) \sim \epsilon^{3\beta-1}, \qquad \epsilon \ll 1, \tag{F 40}$$

where β is given by (F 6); thus,

$$\Gamma_3 \approx \epsilon_{\min}^{3\beta-2}, \qquad \epsilon_{\min} \ll v_L, \tag{F 41}$$

for an unretarded van der Waals potential (5.4).

F.3. *Brownian motion*

The asymptotic approximation (5.21) for weak surfactant diffusion and weak van der Waals attraction was obtained following the analysis described in § F.1.1. Accordingly, integral (5.20) is represented as

$$I_B = I_1 + I_2, \tag{F 42}$$

where I_1 and I_2 are given by (F 9) and (F 10), with

$$f_0(\epsilon) = \frac{2}{(2+\epsilon)^2 G_0(R)}, \tag{F 43}$$

and $g(\epsilon/\epsilon^*)$ dependent on the lubrication cutoff mechanism. For weak surfactant diffusion ($\Lambda \ll 1$) and no van der Waals attraction, $g(\epsilon/\epsilon^*)$ is defined by (F 3) with lubrication cutoff (5.8); for weak unretarded van der Waals attraction (5.4) ($A_H/kT \ll 1$) and no surfactant diffusion,

$$g(\epsilon/\epsilon^*) = \exp\left(-\frac{\epsilon^*}{12\epsilon}\right) \tag{F 44}$$

with cutoff (5.22). Asymptotic behaviours (F 4) and (F 5) hold, with $\beta = 4$. Thus, (5.21) with $\Gamma_4 = \frac{1}{4}(C_1 + C_2)$ is obtained using (F 12)–(F 13).

REFERENCES

Aris, R. 1965 *Vectors, Tensors, and the Basic Equations of Fluid Mechanics*. Prentice-Hall.

Arp, P. A. & Mason, S. C. 1977 The kinetics of flowing dispersions VIII. doublets of rigid spheres (theoretical). *J. Colloid Interface Sci.* **61**, 21–43.

Batchelor, G. K. & Green, J. T. 1972*a* The determination of the bulk stress in a suspension of spherical particles to order c^2. *J. Fluid Mech.* **56**, 401–427.

Batchelor, G. K. & Green, J. T. 1972*b* The hydrodynamic interaction of two small freely-moving spheres in a linear flow field. *J. Fluid Mech.* **56**, 375–400.

Bławzdziewicz, J., Cristini, V. & Loewenberg, M. 1999 Stokes flow in presence of planar interface covered with incompressible surfactant. *Phys. Fluids* **11**, 251–258.

Chen, J. & Stebe, K. J. 1996 Marangoni retardation of the terminal velocity of a settling droplet: The role of surfactant physico-chemistry. *J. Colloid Interface Sci.* **178**, 144–155.

Cichocki, B. & Felderhof, B. U. 1988 Short-time diffusion coefficients and high frequency viscosity of dilute suspensions of spherical Brownian particles. *J. Chem. Phys.* **89**, 1049–1054.

Cichocki, B., Felderhof, B. U., Hinsen, K., Wajnryb, E. & Bławzdziewicz, J. 1994 Friction and mobility of many spheres in Stokes flow. *J. Chem. Phys.* **100**, 3780–3790.

Cichocki, B., Felderhof, B. U. & Schmitz, R. 1988 Hydrodynamic interactions between two spherical particles. *PhysicoChem. Hydrodyn.* **10**, 383–403.

Cristini, V., Bławzdziewicz, J. & Loewenberg, M. 1998 Near-contact motion of surfactant-covered spherical drops. *J. Fluid Mech.* **366**, 259–287.

Edmonds, A. R. 1960 *Angular Momentum in Quantum Mechanics*. Princeton University Press.

Edwards, D., Brenner, H. & Wasan, D. 1991 *Interfacial Transport Processes and Rheology*. Butterworth-Heinemann.

Frumkin, A. N. & Levich, V. G. 1947 *Zhur. Fiz. Khim.* **21**, 1183.

Hamaker, H. C. 1931 The London–van der Waals attraction between spherical particles. *Physica* **4**, 1058–72.

Hocking, L. M. 1973 The effect of slip on the motion of a sphere close to a wall and of two adjacent spheres. *J. Engng Maths* **7**, 207–221.

Jeffrey, D. J. 1982 Low-Reynolds-number flow between converging spheres. *Matematika* **29**, 58–66.

Kim, S. & Karrila, S. J. 1991 *Microhydrodynamics: Principles and Selected Applications*. Butterworth-Heinemann.

Kralchevsky, P., Danov, K. & Ivanov, I. 1996 Thin liquid film physics. In *Foams.* Surfactant Science Series vol. 57 (ed. R. Prud'homme & S. Khan), pp. 1–98. Marcel Dekker.

Landau, L. D. & Lifshitz, E. M. 1987 *Fluid Mechanics*. Pergamon.

Levich, V. G. 1962 *Physicochemical Hydrodynamics*. Englewood Cliffs: Prentice–Hall.

Maldarelli, C. & Huang, W. 1996 The effect of surfactants on the motion of bubbles and drops. In *Flow of Particles in Suspensions.* CISM Courses and Lectures No. 370 (ed. U. Schaflinger), pp. 125–160. Springer.

O'Neill, M. E. & Stewartson, K. 1967 On the slow motion of a sphere parallel to a nearby plane wall. *J. Fluid Mech.* **27**, 705–724.

Pawar, Y. & Stebe, K. J. 1996 Marangoni effects on drop deformation in an extensional flow: The role of surfactant physical chemistry. I. Insoluble surfactants. *Phys. Fluids* **8**, 1738–1751.

Reed, L. D. & Morrison, F. A. 1974 Particle interactions in viscous flow at small values of Knudsen number. *J. Aerosol Sci.* **5**, 175–189.

Schmitz, R. & Felderhof, B. U. 1978 Creeping flow about a sphere. *Physica* A **92**, 423–437.

Spielman, L. A. 1970 Viscous interactions in Brownian coagulation. *J. Colloid Interface Sci.* **33**, 562–571.

Stebe, K. J. & Maldarelli, C. 1994 Remobilizing surfactant retarded fluid particle interfaces. 2. Controlling the surface mobility at interfaces of solutions containing surface-active components. *J. Colloid Interface Sci.* **163**, 177–189.

Stone, H. A. & Leal, L. G. 1990 The effects of surfactants on drop deformation and breakup. *J. Fluid Mech.* **220**, 161–186.

Vlahovska, P. M., Bławzdziewicz, J. & Loewenberg, M. 1998 Rheology of a dilute dispersion of surfactant-covered spherical drops. *Bull. Am. Phys. Soc.* **43**, 2022.

Wang, H., Zinchenko, A. Z. & Davis, R. H. 1994 The collision rate of small drops in linear flow fields. *J. Fluid Mech.* **265**, 161–188.

Yon, S. & Pozrikidis, C. 1998 A finite-volume/boundary-element method for flow past interfaces in the presence of surfactants, with application to shear flow past a viscous drop. *Computers Fluids* **27**, 879–902.

Zhang, X. & Davis, R. H. 1991 The rate of collisions due to Brownian or gravitational motion of small drops. *J. Fluid Mech.* **230**, 479–504.

Zinchenko, A. Z. 1982 Calculations of the effectiveness of gravitational coagulation of drops with allowance for internal circulation. *J. Fluid Mech.* **46**, 58–65.

Zinchenko, A. Z. 1984 Effect of hydrodynamic interactions between the particles on the rheological properties of dilute emulsions. *Prikl. Matem. Mekhan.* **47**, 56–63.

Zinchenko, A. Z. & Davis, R. H. 1994 Gravity-induced coalescence of drops at arbitrary Péclet numbers. *J. Fluid Mech.* **280**, 119–148.